LM-04K001
January 29, 2004

GaInAsSb / AlGaAsSb / GaSb Thermophotovoltaic Devices

CA Wang

NOTICE

GaInAsSb/AlGaAsSb/GaSb Thermophotovoltaic Devices

M.I.T. Technical Seminar

4 February 2004

C.A. Wang

Lincoln Laboratory, Massachusetts Institute of Technology

Lexington, MA

This work was sponsored by the Department of Energy under Air Force Contract No. F19628-00-C-0002. The opinions, interpretations, conclusions and recommendations are those of the author and are not necessarily endorsed by the United States Government.

Viewgraph 1:

Thermophotovoltaic (TPV) devices based on III-V semiconductor alloys with bandgap energies corresponding to the mid-infrared wavelength range 2.2 to 2.5 μm (0.5 to 0.56 eV) are being developed. To date, the highest performing TPV devices in this wavelength range have been achieved for devices based on GaInAsSb and AlGaAsSb alloys lattice matched to GaSb substrates. The first 0.55-eV TPV cells in this materials system were reported at the Third NREL Conference on Thermophotovoltaic Generation of Electricity in 1997. Smaller-bandgap TPV devices have subsequently been reported with concurrent improvements in TPV device performance. This has largely been due to ongoing efforts to understand fundamental processes in materials growth, intrinsic materials properties, and their relationships to TPV device structure design and performance. This work reports some of the fundamental as well as practical issues that have been identified as critical parameters for achieving high performance TPV cells.

This work was sponsored by the Department of Energy under Air Force Contract No. F19628-00-C-0002. The opinions, interpretations, conclusions and recommendations are those of the author and are not necessarily endorsed by the United States Government.

Outline

- Current status of GaInAsSb/AlGaAsSb/GaSb TPV devices
- Materials and device fabrication studies
  - Critical issues for epitaxial growth of GaSb-based materials
  - Materials properties
  - Contact metallization and cell edge treatment
- TPV device structure improvements
  - Integrated distributed Bragg reflectors (DBR)
  - Back surface reflector (BSR)
  - New concepts: wafer-bonded TPVs with internal BSR
- Summary

Viewgraph 2:

The presentation will discuss several aspects of the development of lattice-matched GaInAsSb TPV devices. The growth of device structures, which consist of GaSb, GaInAsSb and AlGaAsSb layers grown epitaxially on GaSb substrates is first presented. A high degree of control and reproducibility is required for producing materials and device structures with high quality, and this is demonstrated for structures grown by organometallic vapor phase epitaxy (OMVPE). The performance of TPV devices and new structures is presented.

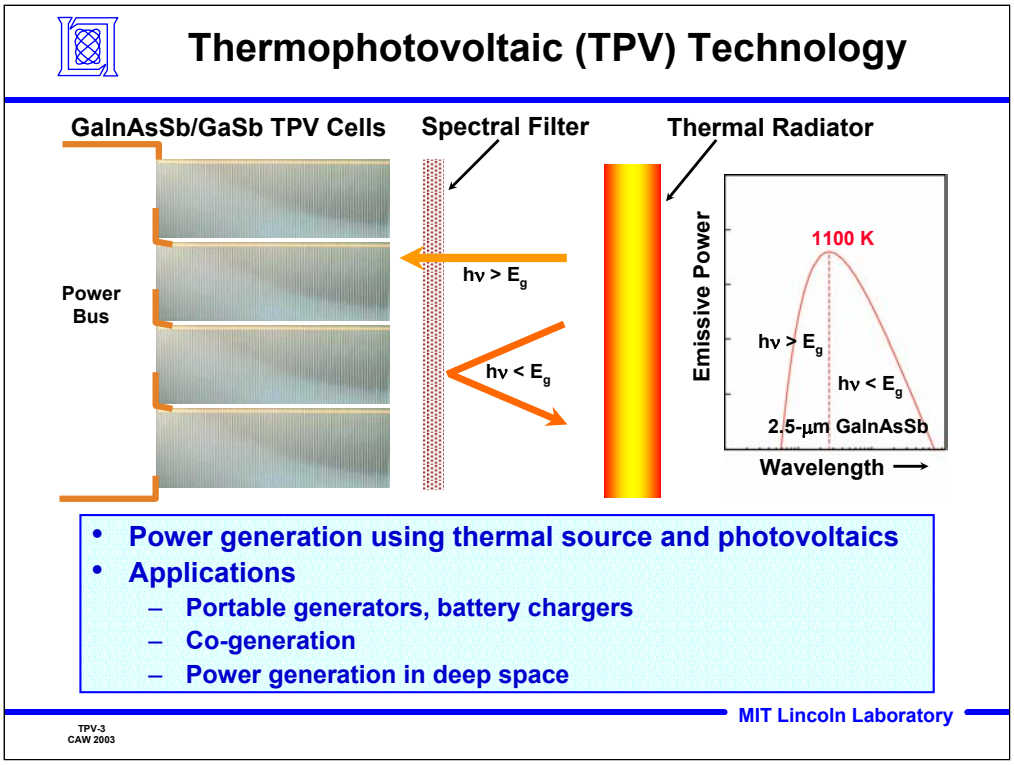

Viewgraph 3:

The main thrust of our work is on thermophotovoltaics, which are a subset of photovoltaics. Thermophotovoltaic technology involves the conversion of thermal energy to electrical energy through photovoltaic cells. The system consists of a thermal radiator, spectral filters which reflect below bandgap photons back to the radiator, and photovoltaic cells. Since the thermal radiator is heated to a temperature between 1100 and 1700 K, the most effective materials for the photovoltaic cell will have an energy gap that corresponds to the wavelength range between 2 and 2.5 μm, i.e. the GaInAsSb alloys.

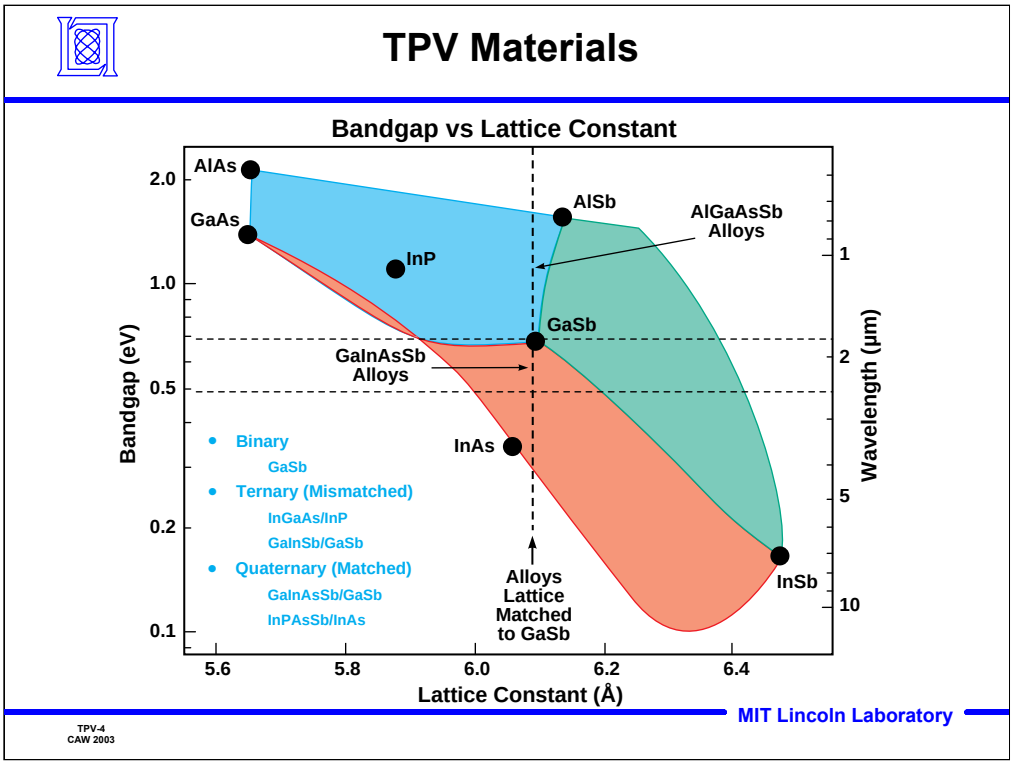

Viewgraph 4:

Several III-V materials systems with energy gaps between 0.5 and 0.6 eV are being developed for TPV devices for use in systems with low-temperature emitters (1100 K). The graph on the left shows the energy gap vs lattice constant for III-V semiconductors that can meet this requirement. Both lattice-mismatched ternary (InGaAs/InP) and lattice-matched quaternary (GaInAsSb/GaSb) alloys have been used in high performance TPV cells.

This work focuses on GaInAsSb and AlGaAsSb quaternary alloys lattice matched to GaSb substrates. A significant advantage of these lattice-matched alloys is the versatility in obtaining alloys with a large range of energy gaps from 0.3 eV for InAsSb to nearly 2 eV for AlAsSb.

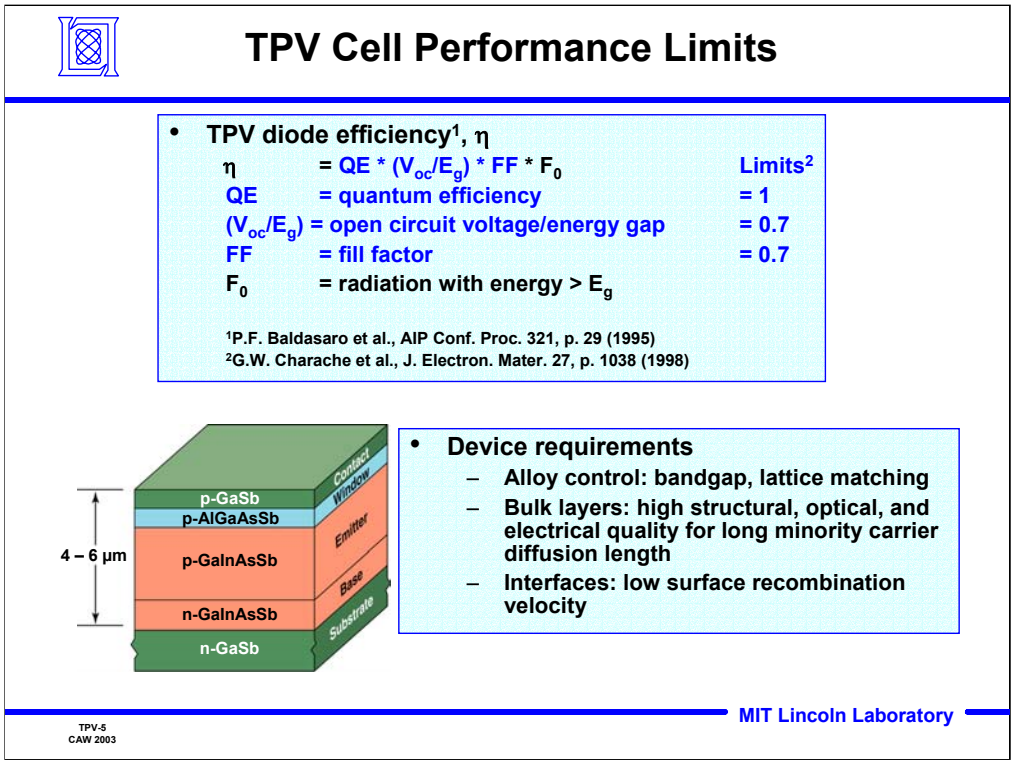

Viewgraph 5:

The radiator-to-electric efficiency for a TPV cell can be described by the expression shown in the viewgraph. The parameters that are specifically related to TPV cell performance are QE, V_{oc}, E_g, and FF. Thus, to maximize system efficiency, the epitaxial device structure must be optimized according to these parameters. Consequently, to the extent that the materials and device structure can be developed, this work has studied (1) properties of bulk layers in order to achieve maximum minority diffusion lengths and (2) heterointerfaces in order to minimize surface recombination velocity. The quaternary alloy composition, which determines the bandgap, is lattice matched to the substrate.

The present design of the TPV device structure is a p-on-n configuration, since shallow p-type ohmic contacts are more readily achieved compared to shallow n-type contacts. The absorption coefficient of GaInAsSb near the band-edge is only about half of that of GaAs, and therefore a thick p-type GaInAsSb emitter layer is used as the absorption layer. Generation of carriers in this layer is preferable since it has a higher minority carrier diffusion length compared to n-type GaInAsSb. A critical layer in the structure is the AlGaAsSb window layer which reduces the interface/surface recombination velocity. A GaSb window has also been used with success.

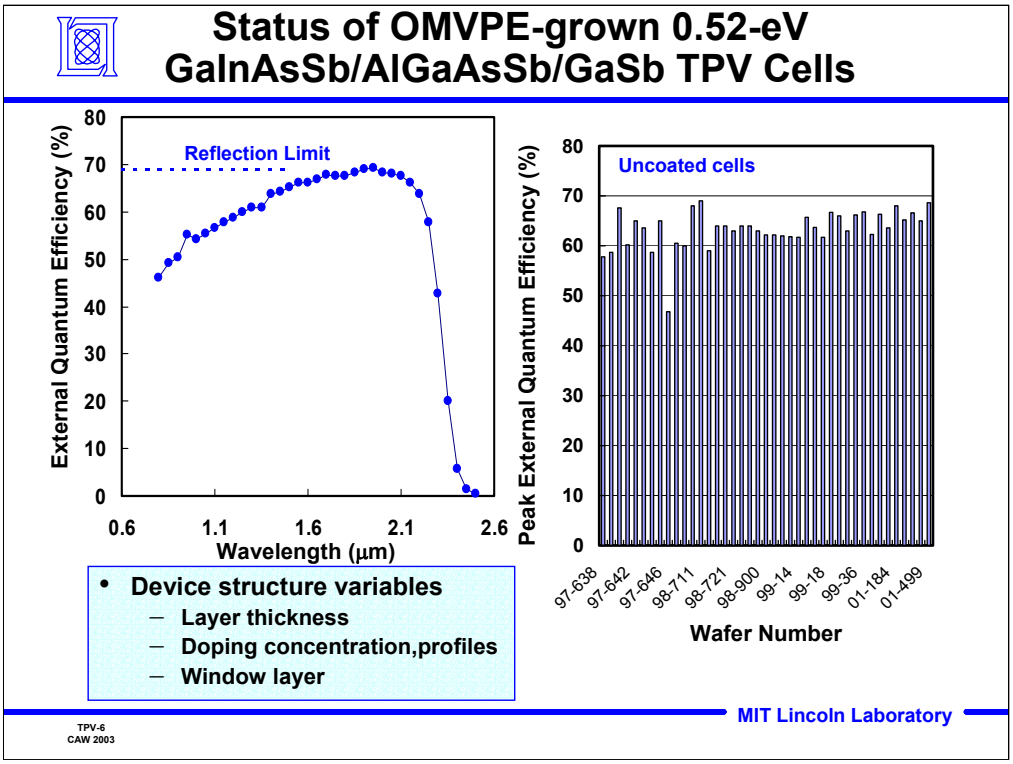

Viewgraph 6:

The performance of typical TPV devices is presented. The spectral response of an uncoated 0.52-eV TPV device with AlGaAsSb window layer is shown on the left. The external quantum efficiency (EQE) for the uncoated device is approaching the theoretical limit. The EQE decreases below 1.7 μm due to absorption in the GaSb/AlGaAsSb layers and drops off below 20% at 2.4 μm. This bar chart on the right summarizes the peak value of the EQE for TPV cells fabricated from all TPV device structures grown over a period of several years. The structures are not the same, and layer emitter layer thickness and doping or window layers were varied. The results show the peak value of the EQE is reasonably insensitive to the device structure. TPV devices with cutoff wavelengths, the wavelength where the EQE is 50% of its peak value, out to 2.5 μm have been measured with similarly high EQE.

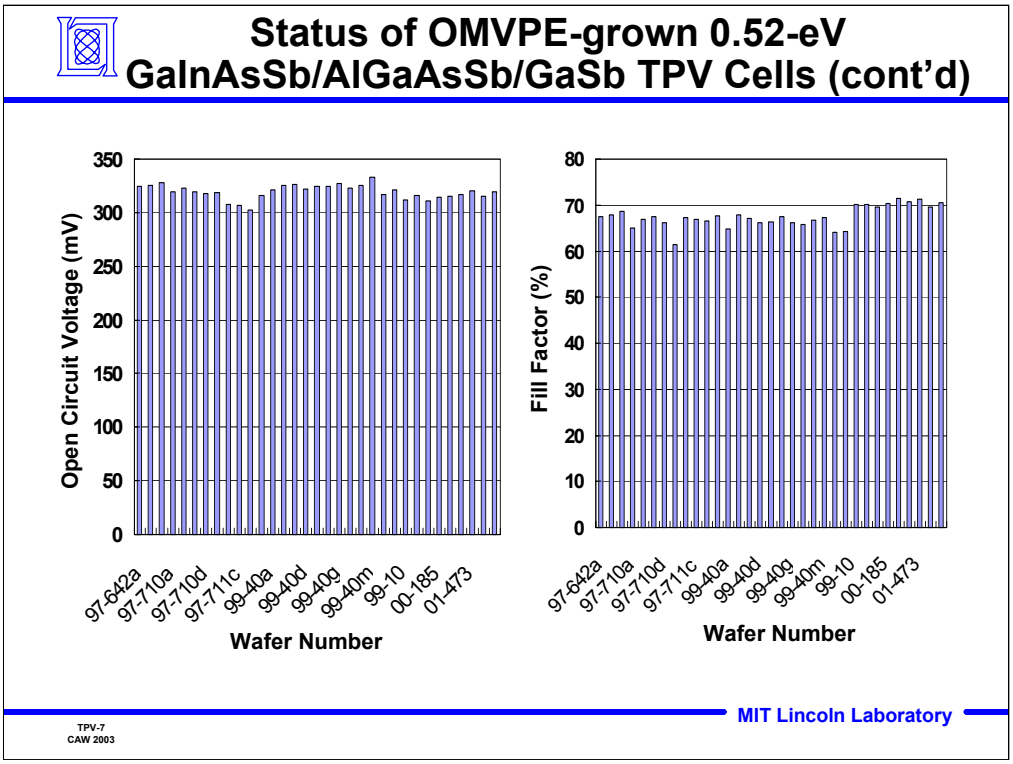

Viewgraph 7:

Similarly, TPV cells fabricated from numerous TPV wafers exhibit open circuit voltages (V_{oc}) that typically exceed 300 mV and are as high as 327 mV. Fill factors (FF) as high as 70% have been measured.

The efficiency and FF performance of GaInAsSb cells are approaching theoretical limits. Improvements can still be made in V_{oc} through the reduction in the diode dark current.

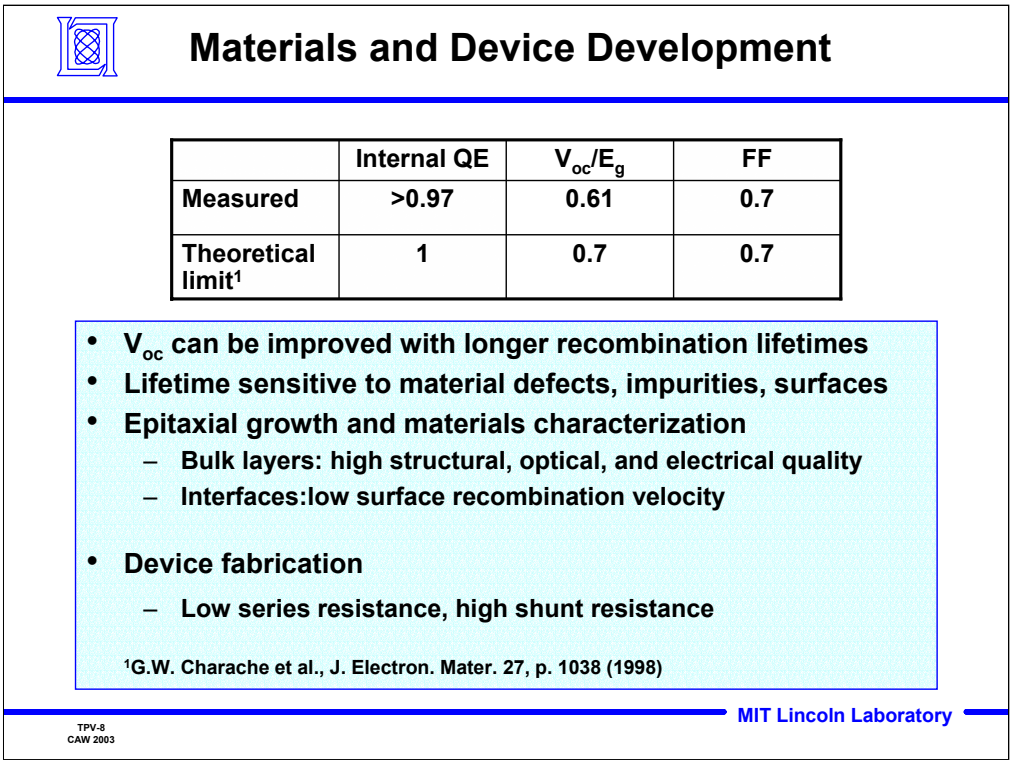

Viewgraph 8:

Extensive materials and device issues that have been considered in the development of TPV cells are listed in this viewgraph. Several of these topics are individually addressed in the presentation. Further increases in V_{oc} require further in-depth analysis of fundamental issues for further device improvement.

Materials and Device Development

- OMVPE of GaSb/GaInAsSb/AlGaAsSb
  - GaSb substrates
  - Growth of low-bandgap metastable GaInAsSb alloys
  - n- and p-type doping GaSb/GaInAsSb
- Materials characterization
  - Microstructural properties
  - Minority carrier lifetime
    - Carrier mobility, photoreflectance, photoconductivity, photoluminescence
  - Surface/interface recombination
- TPV device structures
  - Optimization of layer structure and interfaces
  - Structure enhancements for photon recycling
- TPV device processing
  - Contacts for low series resistance, sidewall treatment for high shunt resistance

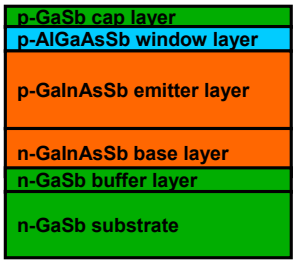

Viewgraph 9:

Optimizing TPV device performance requires insight into numerous materials growth, device design, and device fabrication and testing. Topic areas are listed in this viewgraph. This talk will focus on the critical issues in materials growth and device fabrication.

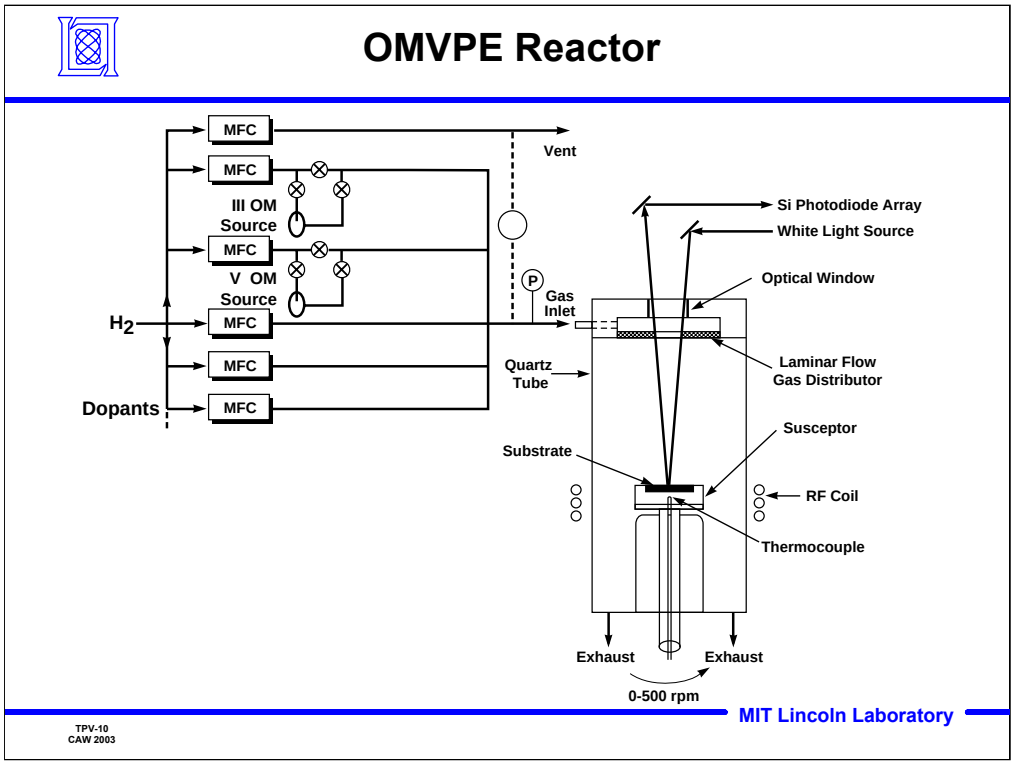

Viewgraph 10:

The epilayers are grown by OMVPE in a vertical rotating-disk reactor. All organometallic sources are used, and precise metering of the sources is achieved with mass flow controllers. The susceptor is heated by radio frequency, and epitaxial growth is monitored with in-situ reflectance .

The reflectance set-up shown here is in a near-normal configuration, and requires an optical window at the top of the reactor. Since the reactants are introduced here, a less obtrusive reflectance configuration directs light through the sides of the quartz reactor tube. In-situ reflectance is presently performed at 55° from the substrate normal.

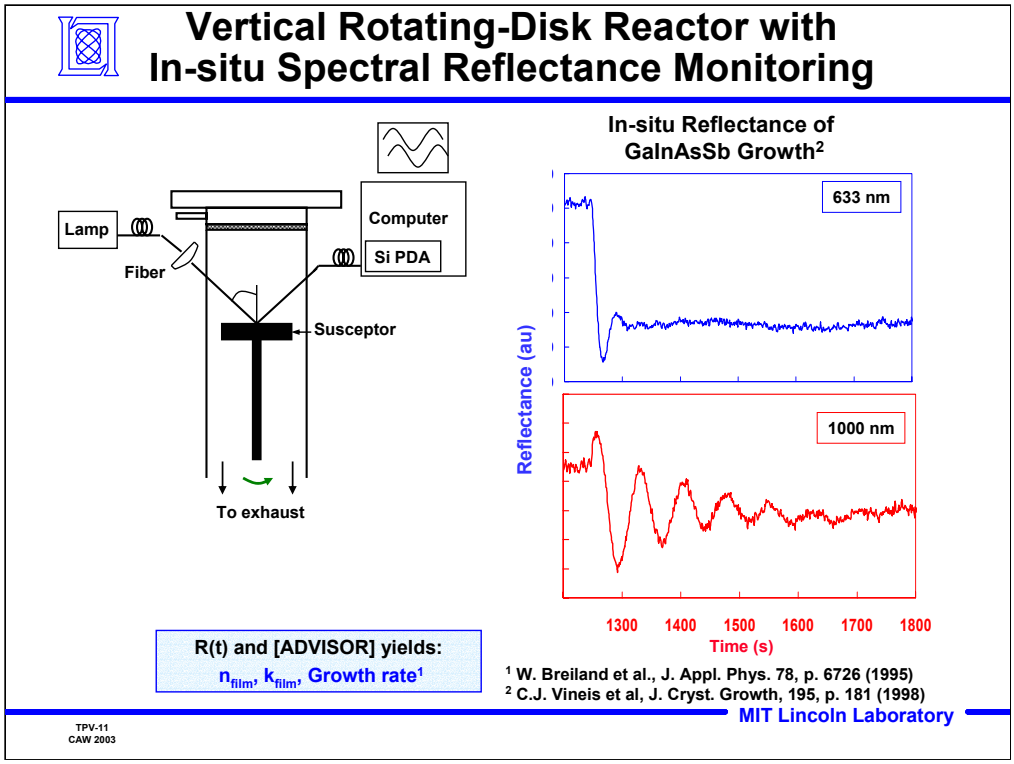

Viewgraph 11:

In-situ spectral reflectance monitoring has been shown to be useful for studying oxide desorption from substrates and for determining growth rates and alloy composition. Furthermore, reflectance can be used to monitor the stability of the growth surface. The advantage of spectral reflectance over a single wavelength is that the most sensitive wavelength for a given material is used for data analysis. The graphs on the right show reflectance at 633 and 1000 nm for growth of GaInAsSb. There is more absorption in the reflectance at 633 nm than that at 1000 nm: only the data at 1000 nm can be used to accurately determine the GaInAsSb growth rate. However, for studies with growth interruptions, a monitoring wavelength of 633 nm was determined to be the most suitable because it had the highest signal to noise ratio.

GaSb Substrate Issues

- **GaSb substrate quality**
  - **Wafer bow**
  - **Surface contamination**
- **Substrate surface preparation for growth**
  - **Epi-ready vs. etched substrate**
  - **Thermal treatment/oxide removal prior to epitaxy**
  - **GaSb vs. GaInAsSb epitaxial growth**

Viewgraph 12:

Growth of high-quality lattice-matched epitaxial layers requires high-quality substrates, which serve as the template for subsequent crystal growth.

Since GaSb-based materials are less developed compared to GaAs- and InP-based materials, the availability of high-quality GaSb substrates has been more limited. The following viewgraphs describe some of the differences observed in the quality of substrates as-received from vendors. Equally important is preparation of the substrate before epitaxial growth.

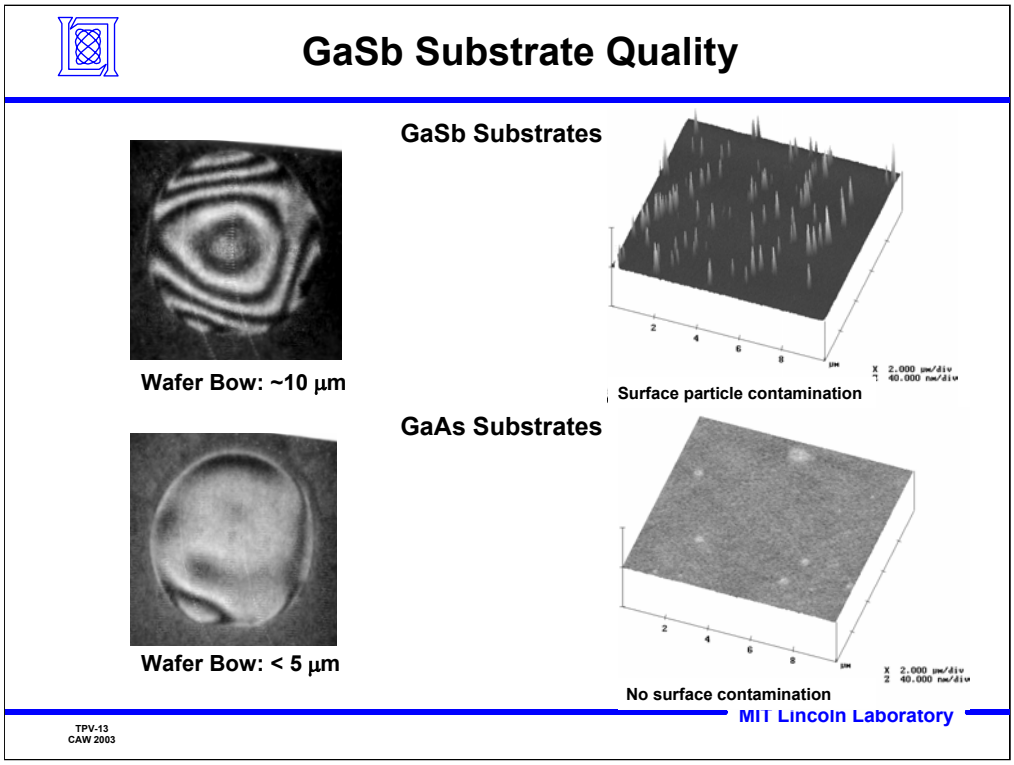

Viewgraph 13:

Two problems of as-received GaSb substrates were identified and are illustrated in this viewgraph. GaSb is a softer material than either GaAs or InP, and as a result, substrates are more susceptible to damage during cutting, lapping, and polishing. The excessive wafer bow in GaSb substrates compared to GaAs substrates is related to residual damage on the back-side of the substrate.

Another problem that was encountered was particle contamination on substrate surfaces. Surface examination of particle size and chemical analysis indicated that the contamination is from SiO_2 polishing particles which become imbedded in the GaSb surface. The particles can result in surface defects in the epitaxy.

GaSb Substrate Preparation

- **GaSb substrate preparation difficult compared to GaAs, InP**
  - **GaSb oxidation rate significantly higher than GaAs, InP**
  - **GaSb oxidation rate at room temp is logarithmic[1]**
  - **Wet-etched GaSb substrates rinsed in 2-propanol**
- **Sb_2O_3 thermodynamically unstable with GaSb[2]**
  - **$Sb_2O_3 + 2GaSb \rightarrow Ga_2O_3 + 4Sb$ $\Delta G = -68.5$ kcal/mol**
  - **GaSb consumed by reaction with Sb_2O_3 even at room temperature**

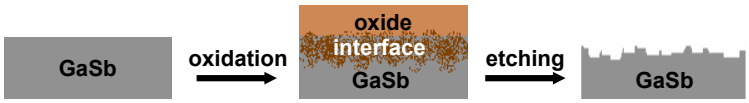

[1]Y. Mizokawa et al., Thin Solid Films 156 (1988) 127
[2]G.P. Schwartz et al., J. Electrochem. Soc. 127 (1980) 1480

Viewgraph 14:

The cleaning and etching of the substrate before epitaxial growth is critical for obtaining high quality epitaxy. All substrates have a native oxide that must be removed before epitaxy, and the GaSb oxidation rate is considerably higher compared to that for more conventional materials such asGaAs or InP. The oxide can be removed either by chemical wet etching or by thermal desorption. Native oxides on GaSb, however, are thermodynamically unstable and GaSb can be consumed in a chemical reaction with the antimony oxide during heating of the GaSb substrate.

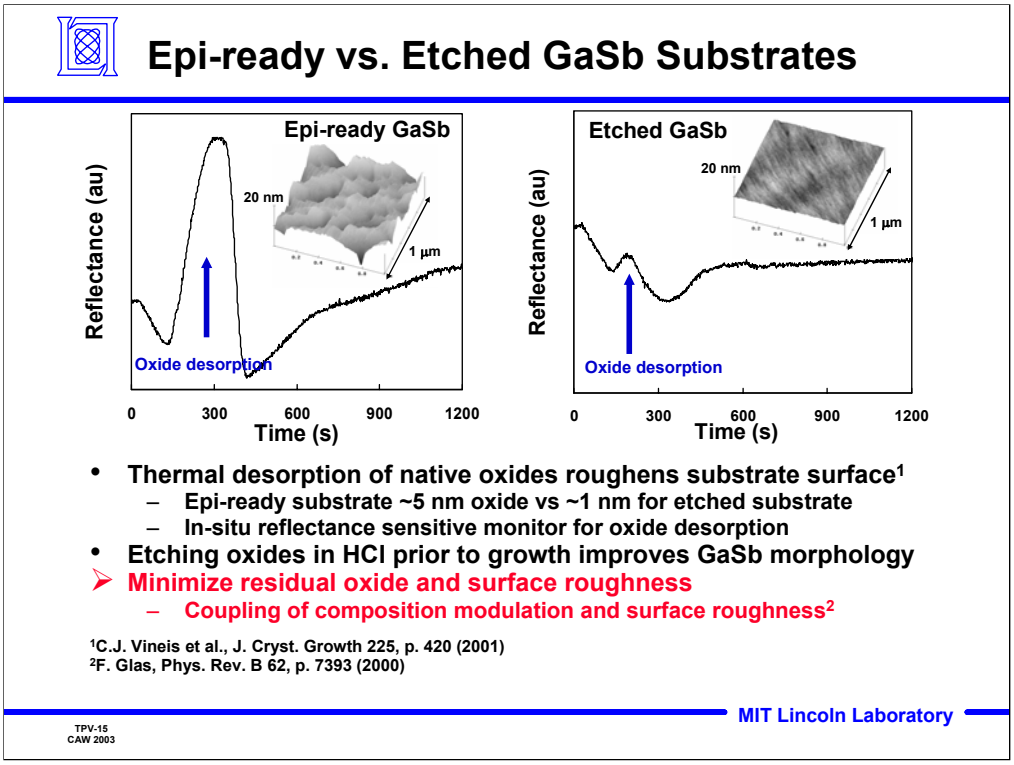

Viewgraph 15:

The oxide removal was studied by in-situ reflectance monitoring. The magnitude of the increase in reflectance at around 250 to 300 s is proportional to the thickness of the oxide layer. The reflectance curves indicate that the oxide is significantly thicker on the epi-ready substrate compared to the etched one.

Atomic force microscopy (AFM) revealed that the surface of the epi-ready substrate after oxide removal was rougher than the etched substrate, which is consistent with the consumption of GaSb during heating of the GaSb substrate and roughening of the substrate surface. Since etching removes the oxide layer, a smoother starting surface before epitaxy can be achieved for these substrates.

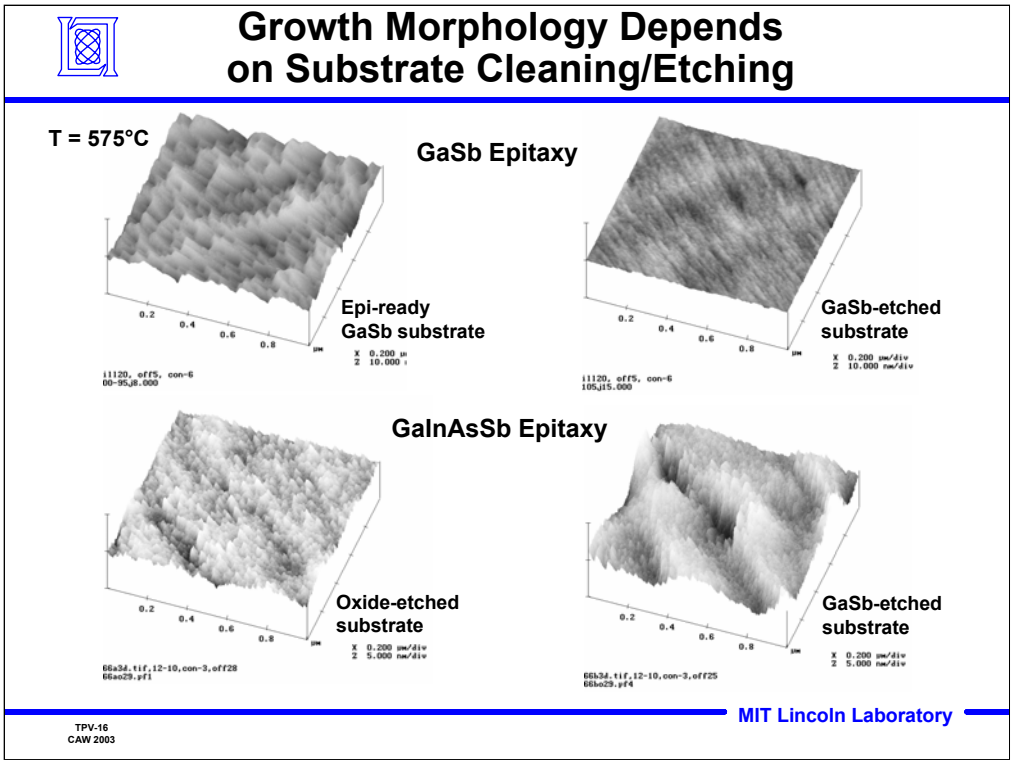

Viewgraph 16:

The surface morphology of GaSb and GaInAsSb epilayers was studied by AFM. In general, the smoother the surface, the better the epitaxial quality.

Oxide removal is a critical step for good growth morphology, and the two top images show that GaSb epitaxy on epi-ready substrates without any etching prior to growth is rougher compared to growth on substrates that were etched in an acetic/bromine based etch. The thick oxide layer on the epi-ready substrate reacts with the GaSb surface and roughens the starting growth surface. The subsequent GaSb growth is rough as this morphology propagates through the epitaxial layer.

Furthermore, it was found that GaInAsSb epitaxy is more sensitive to surface preparation than GaSb. The lower left image shows the morphology for GaInAsSb grown when only the oxide layer was etched away, while the right image is for GaInAsSb grown on an etched substrate such that a few tens of nanometers of GaSb was removed. GaInAsSb on the etched substrate is rougher, suggesting that etching the GaSb substrate introduces some roughening. The GaInAsSb growth is more sensitive to surface roughness because of higher adatom surface diffusion. The importance of adatom diffusion is discussed later in the presentation.

GaInAsSb/AlGaAsSb Materials Issues

- **GaInAsSb: Fundamental limitations of thermodynamically metastable alloys can be mediated by growth kinetics**
  - **Excellent electro-optical properties with low growth temperature (525 °C), high growth rate (5 μm/h), preferred atomic surface structure (substrate misorientation angle and direction, (001) 6°→ (1-11)B)**
- **AlGaAsSb: Affinity of Al-C and Al-O enhances C and O impurity incorporation**
  - **Impurities reduced by altering growth chemistry**
- **Practical limitations of source precursors for OMVPE growth**
  - **Use of alternative source precursors for GaInAsSb and AlGaAsSb: triethylgallium, tritertiarybutylaluminum, solution trimethylindium, tertiarybutylarsine, trimethylantimony**
- **Heterostructure growth of GaInAsSb/AlGaAsSb**
  - **Optimum growth temperatures for GaInAsSb and AlGaAsSb are different**
  - **Growth interruptions affect interface recombination velocity**

Viewgraph 17:

Some of the issues associated with growth of the TPV device structures are discussed.

GaInAsSb alloys of interest for 0.5- to 0.6 eV-TPV devices are thermodynamically metastable and can phase separate into regions that are inhomogeneous in composition. In general, inhomogeneity can degrade material structural and electro-optical quality, and thus reduce minority carrier properties. OMVPE growth is a non-equilibrium process, and kinetics can effectively limit phase separation. Parameters such as growth temperature, growth rate, and atomic surface stucture were studied, and conditions that yield high quality epitaxial GaInAsSb are listed above.

AlGaAsSb alloys are used as a window layer in the TPV device structure. Impurities such as carbon and oxygen can be problematic with conventional growth precursors. However, some of the practical limitations of growing both of these alloys have been overcome by the use of alternative precursors, and a high degree of controllability and reproducibility is achieved.

The interfaces in heterostructures are critical in TPV cells since surface/interface recombination velocity is a controlling parameter in quantum efficiency and open circuit voltage. The characterization of interfacial growth is thus important for optimizing device performance.

GaInAsSb OMVPE Materials

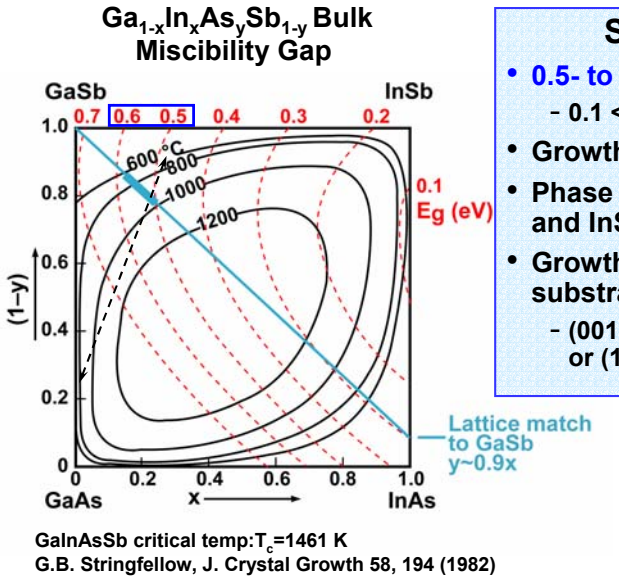

GaInAsSb critical temp: T_c=1461 K
G.B. Stringfellow, J. Crystal Growth 58, 194 (1982)

Sample details

- 0.5- to 0.6-eV GaInAsSb/GaSb
  - 0.1 < x,y < 0.2
- Growth temp 525-575 °C
- Phase separation into GaAs- and InSb-rich regions
- Growth on vicinal GaSb substrates
  - (001) 2 or 6°→ (101), (1-11)B, or (111)A

Viewgraph 18:

The GaInAsSb alloys have a large miscibility gap shown here, and phase separation is a major factor that degrades material quality and degrades device performance. This miscibility diagram shows that GaInAsSb alloys that can be lattice matched to GaSb and have energy gaps below about 0.6 eV are thermodynamically metastable for growth below 600 °C. Since the growth temperatures used for organometallic vapor phase epitaxy (OMVPE) of these alloys is 575 °C and lower, the GaInAsSb alloys in this study are metastable. Consequently, Ga atoms will have a tendency to cluster with the As and the In with Sb. This will result in compositional inhomogeneities and phase separation.

The OMVPE growth process is non-equilibrium, and growth kinetics can be used successfully to limit the extent of phase separation in these alloys. This work investigated several effects including growth temperature, growth rate, and substrate misorientation to establish the best growth conditions for high quality GaInAsSb epilayers. TEM, AFM, XRD, and PL were used to characterize the layers.

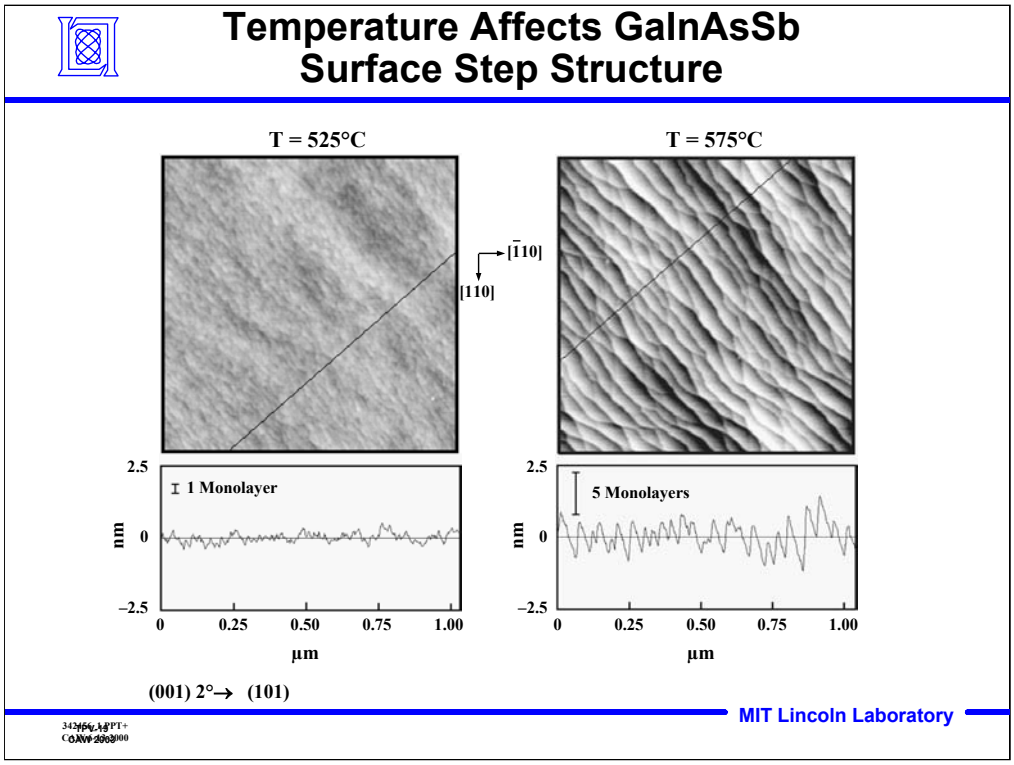

Viewgraph 19:

AFM images of GaInAsSb grown at 525 and 575 °C indicate that the growth mode is by step flow at the lower temperature, while it is step-bunched at the higher temperature. Extensive materials characterization of epilayers grown at temperatures between 525 and 575 °C suggest that the step-flow growth mode is preferred to minimize phase separation. Such a growth mode minimizes adatom surface diffusion.

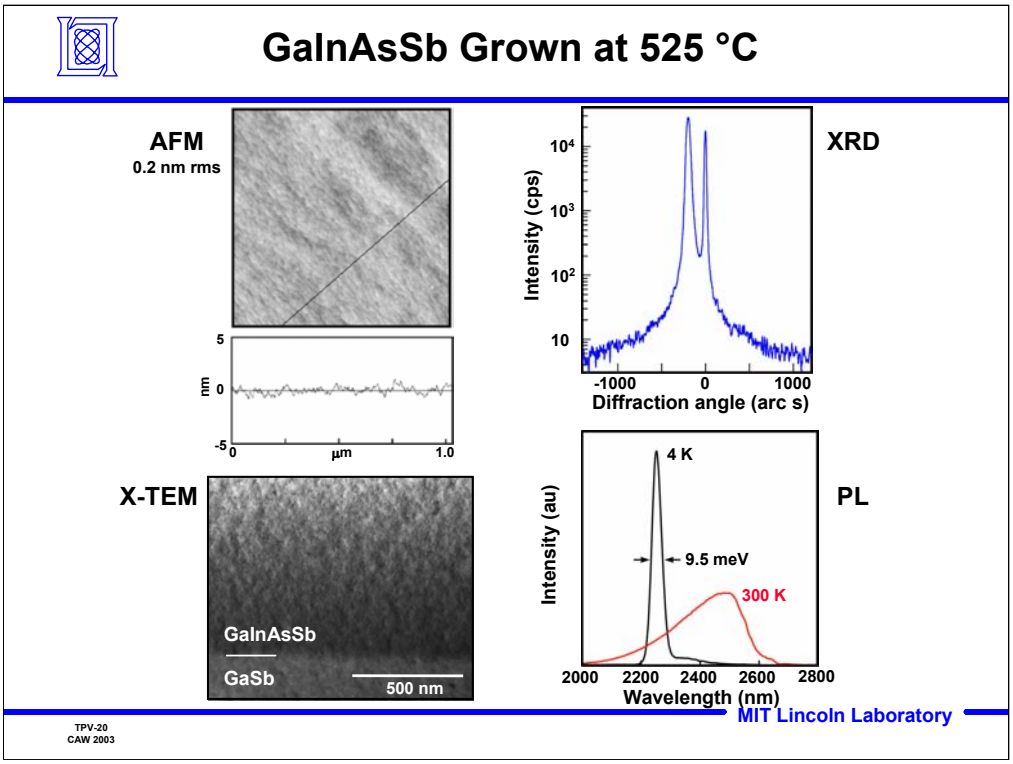

Viewgraph 20:

This viewgraph shows AFM, x-ray diffraction (XRD), cross-section transmission electron microscopy (TEM), and photoluminescence (PL) characterization of GaInAsSb with high materials quality. The narrow full-width at half-maximum (FWHM) of XRD and PL, and the minimal contrast in TEM are indicative of uniform material

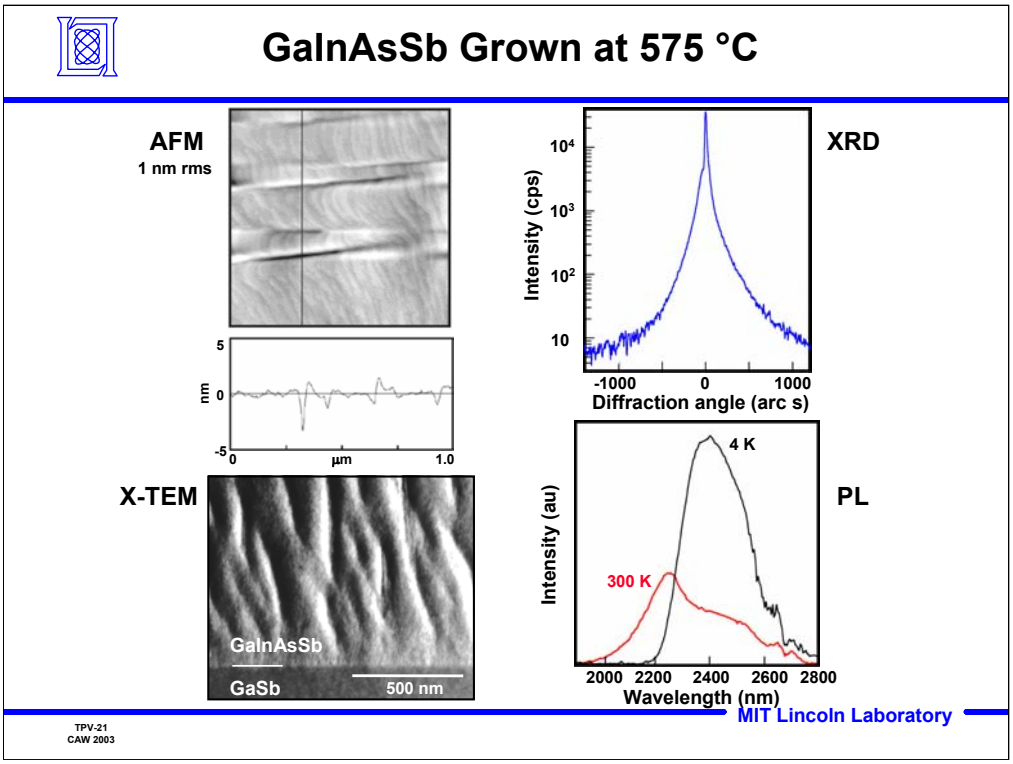

Viewgraph 21:

Conversely, the GaInAsSb material quality clearly shows considerable compositional non-uniformity and degradation in all the materials properties.

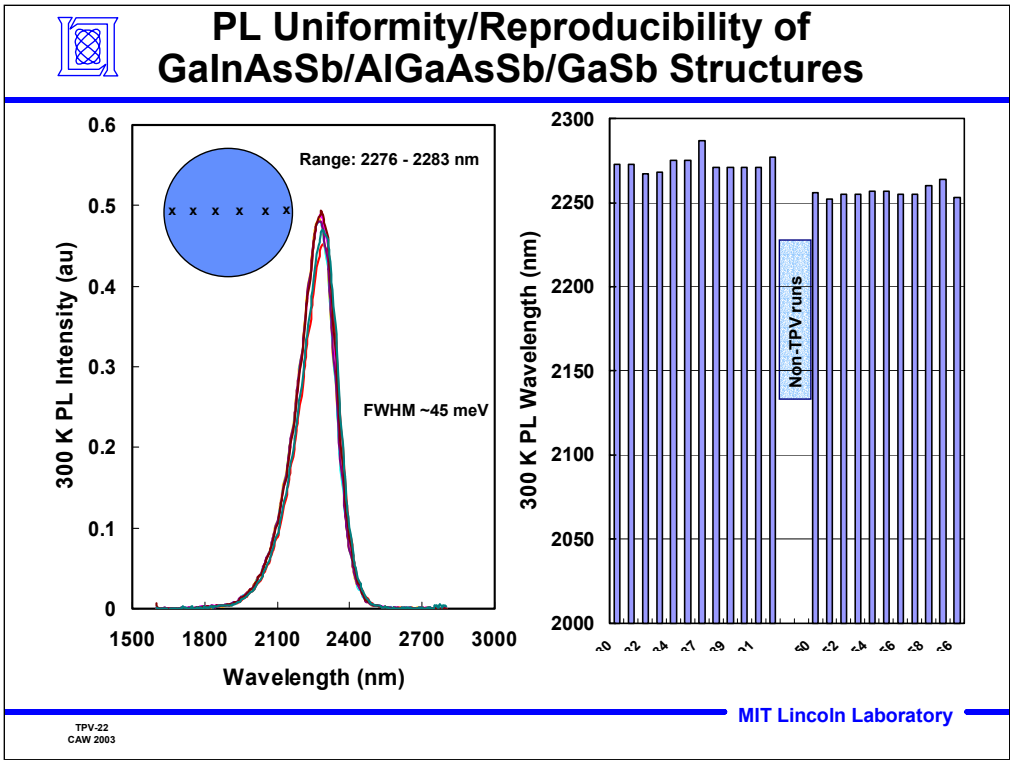

Viewgraph 22:

Macroscopic uniformity was also achieved for GaInAsSb grown under conditions to minimize phase separation. The uniformity and reproducibility of GaInAsSb structures is shown in this viewgraph. The PL emission wavelength (alloy composition) and intensity is very uniform over a 2-inch-diameter substrate. Two separate series of growth runs indicate reproducibility in PL wavelength.

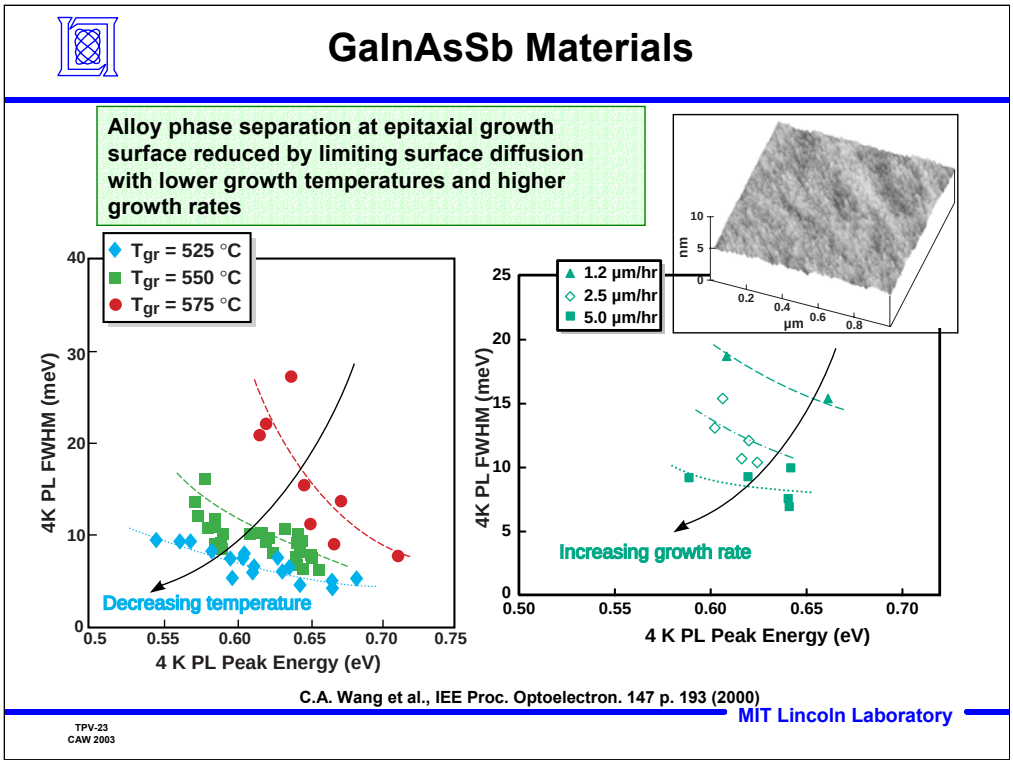

Viewgraph 23:

The FWHM of 4 K PL data of GaInAsSb was used as a measure of material quality and phase separation for undoped GaInAsSb, and data for samples grown under various conditions are summarized in this slide. The results indicate improvements in GaInAsSb layers grown at lower temperatures and higher growth rates. The smallest FWHM value measured is 4.7 meV at 0.643 eV, which is the lowest value that has been reported for this alloy system grown by OMVPE or MBE.

The dominant factor that influences alloy uniformity on the microscale is adatom diffusion on the surface before incorporation into the lattice. Surface diffusion is minimized for lower growth temperatures and higher growth rates. In addition, the substrate misorientation direction and miscut angle was also found to affect crystal quality. The results shown in this viewgraph demonstrate the improvement in GaInAsSb alloys for grown under these conditions. The narrow PL FWHM values are indicative of a high degree of microscopic uniformity.

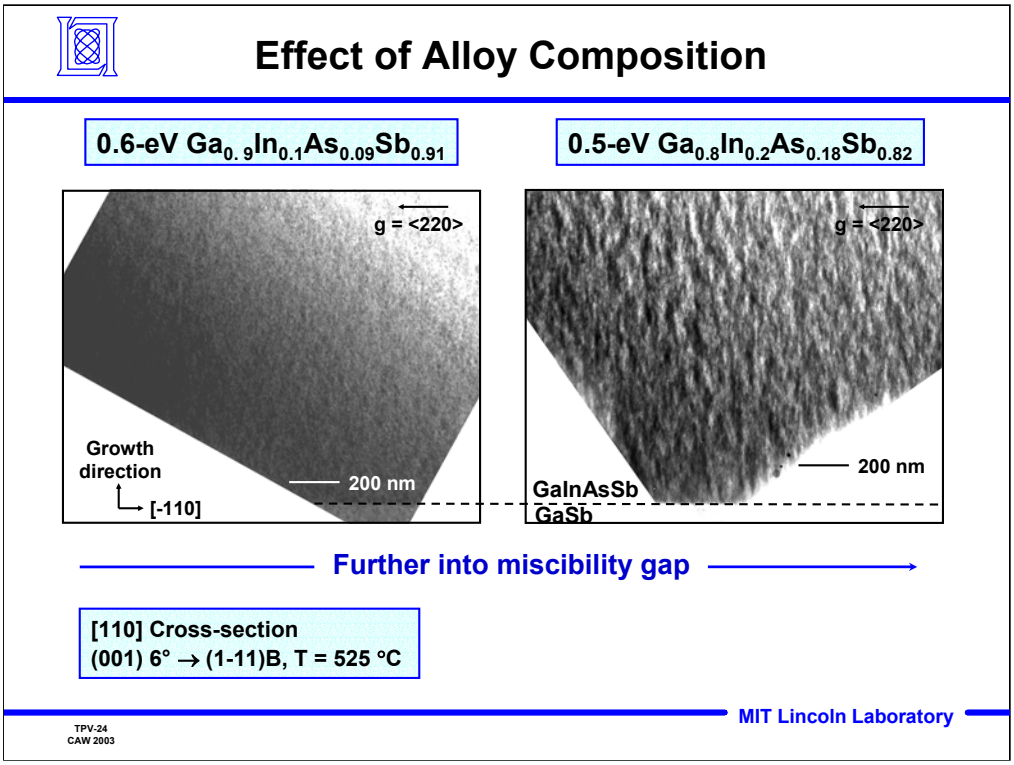

Viewgraph 24:

This viewgraph shows cross-section TEM images of GaInAsSb of different alloy compositions. As the alloy composition penetrates further into the misibility gap, the TEM contrast increases due to spinodal decomposition.

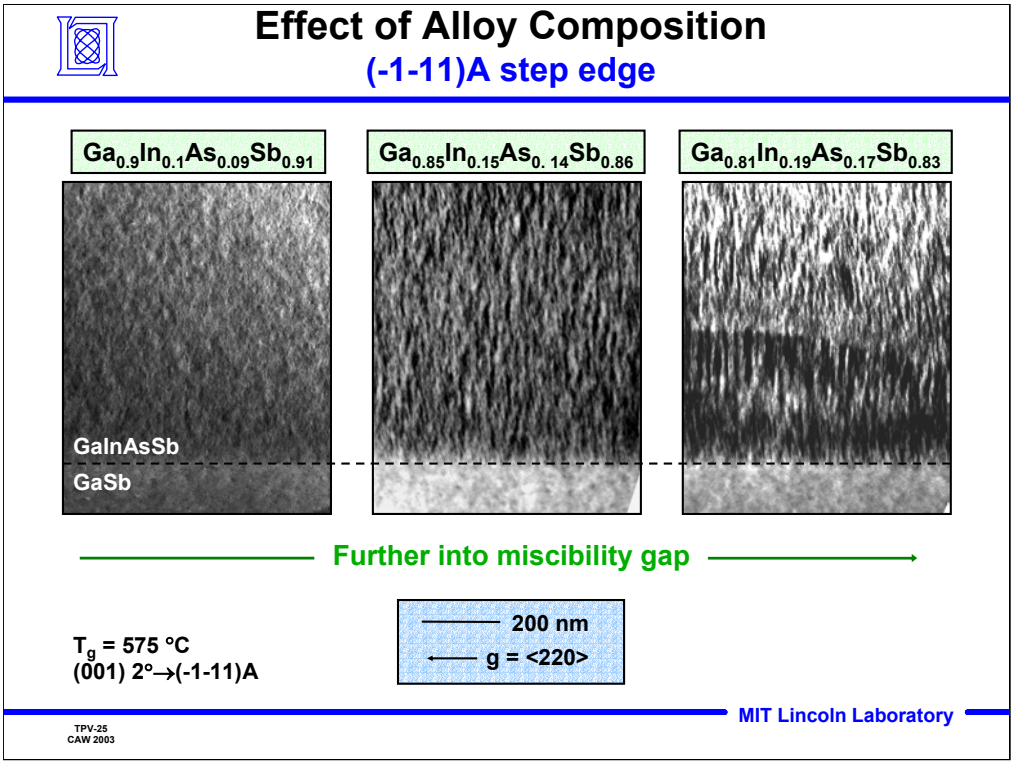

Viewgraph 25:

This viewgraph shows TEM cross-sections of alloys grown on (001) substrates miscut 2° toward (1-11)A. Contrast modulations increase as the alloy composition moves further into the miscibility gap.

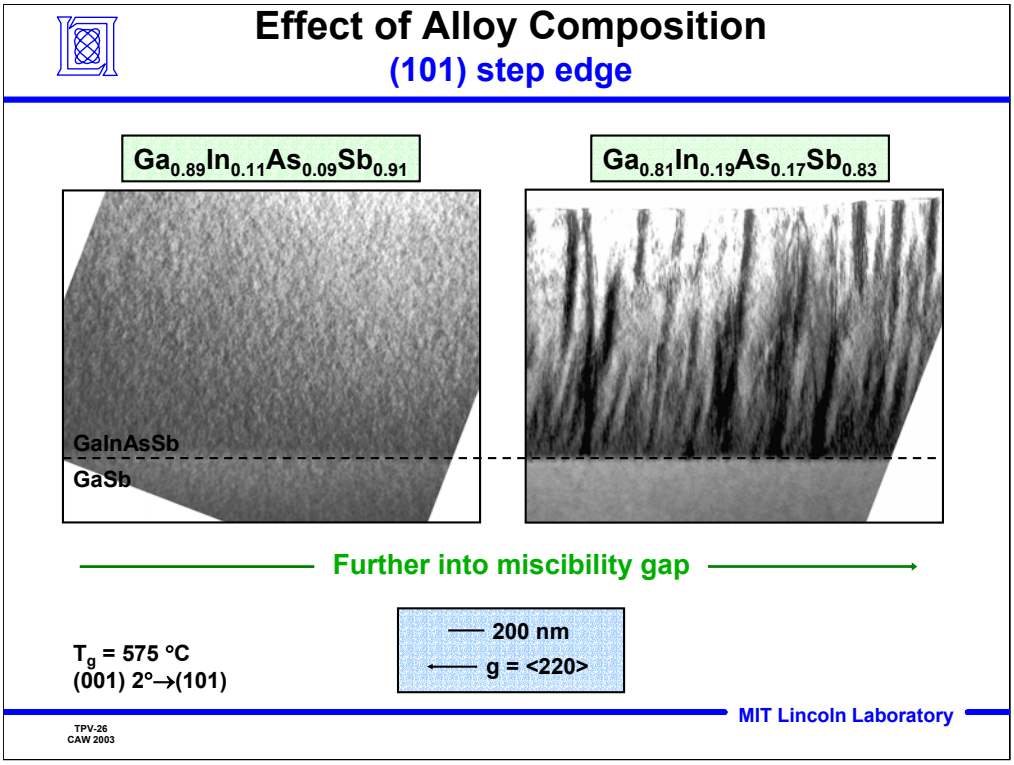

Viewgraph 26:

This viewgraph shows TEM cross-sections of alloys grown on (001) substrates miscut 2° toward (101). Contrast modulations increase as the alloy composition moves further into the miscibility gap. Note that the contrast in the higher alloy layer is greater in this viewgraph compared to the previous two viewgraphs.

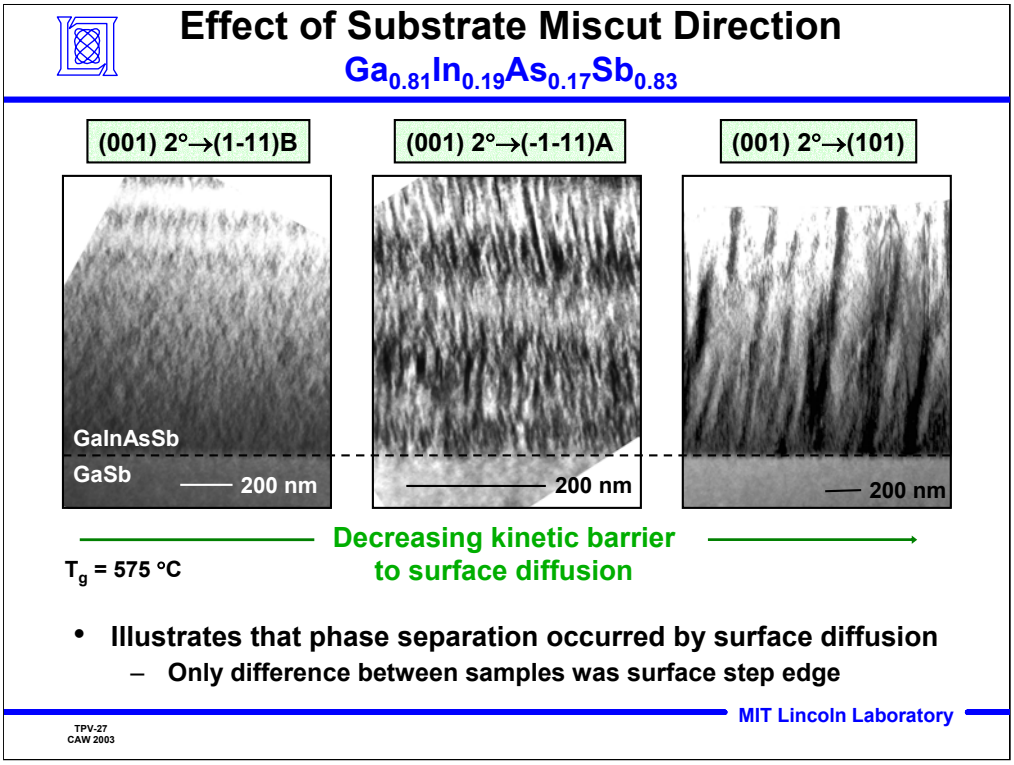

Viewgraph 27:

This viewgraph shows TEM cross-sections of alloys grown on the various miscut substrates. All the layers have a similar alloy composition, and were grown under the same conditions of growth rate, growth temperature and miscut angle. However, they show various contrast modulations. Since the only difference is miscut direction, the bonding/chemistry at step edge is very important in determining phase separation. These results show that phase separation occurs by surface diffusion. Since the adatom diffusion and incorporation is anisotropic, the miscut direction can be critical in determining the extent of phase separation.

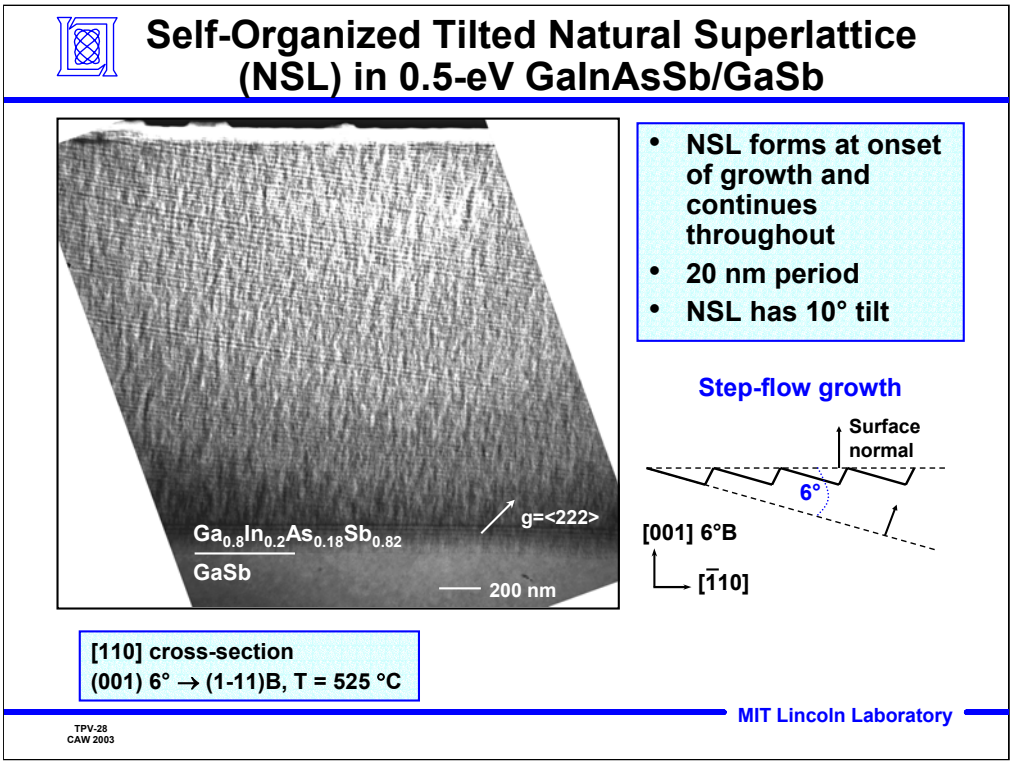

Viewgraph 28:

An interesting self-organized natural superlattice(NSL) was observed in GaInAsSb materials that also showed spinodal-like contrast modulations. This viewgraph contains a cross-section TEM image illustrating the NSL in the GaInAsSb epilayer. The image was obtained using a dark-field, <222> 2-beam condition. The vertical composition modulation exhibits two forms – a 0° variant that is parallel to the epilayer/substrate interface, and a 10° variant that is tilted 10° with respect to the surface normal.

The observed contrast arises from a very small degree of strain associated with a modulation in composition in the vertical direction. The contrast, and thus compositional differences between the layers, depended on the growth conditions and the alloy composition. It was found that the vertical composition modulation can be reduced or enhanced by varying the growth conditions.

Cross-section TEM suggests that GaInAsSb self-organizes at the onset of growth and maintains a consistent periodicity throughout several microns of deposition. A particularly remarkable feature of the vertical modulation is the ordering of atoms to produce a layered structure that is tilted 4° in addition to the miscut angle of the (001) substrate surface plane.

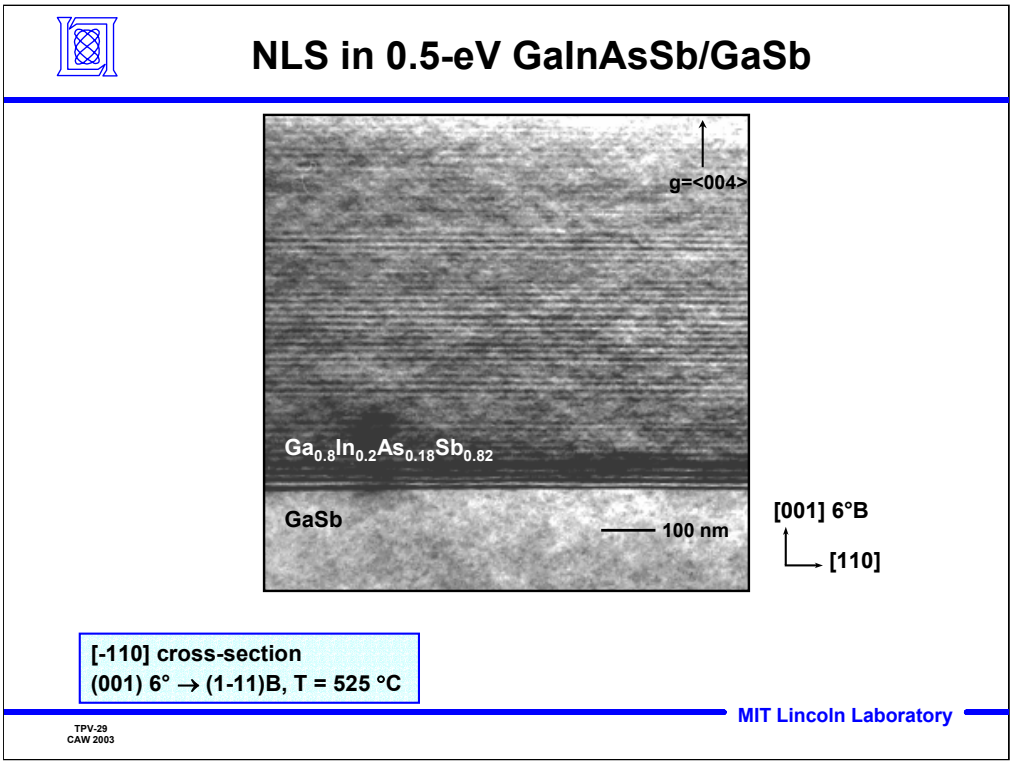

Viewgraph 29:

This viewgraph contains the orthogonal cross-section TEM image illustrating the self-organized NSL in the GaInAsSb epilayer. In this cross-section, the self-organized NSL is parallel to the growth surface.

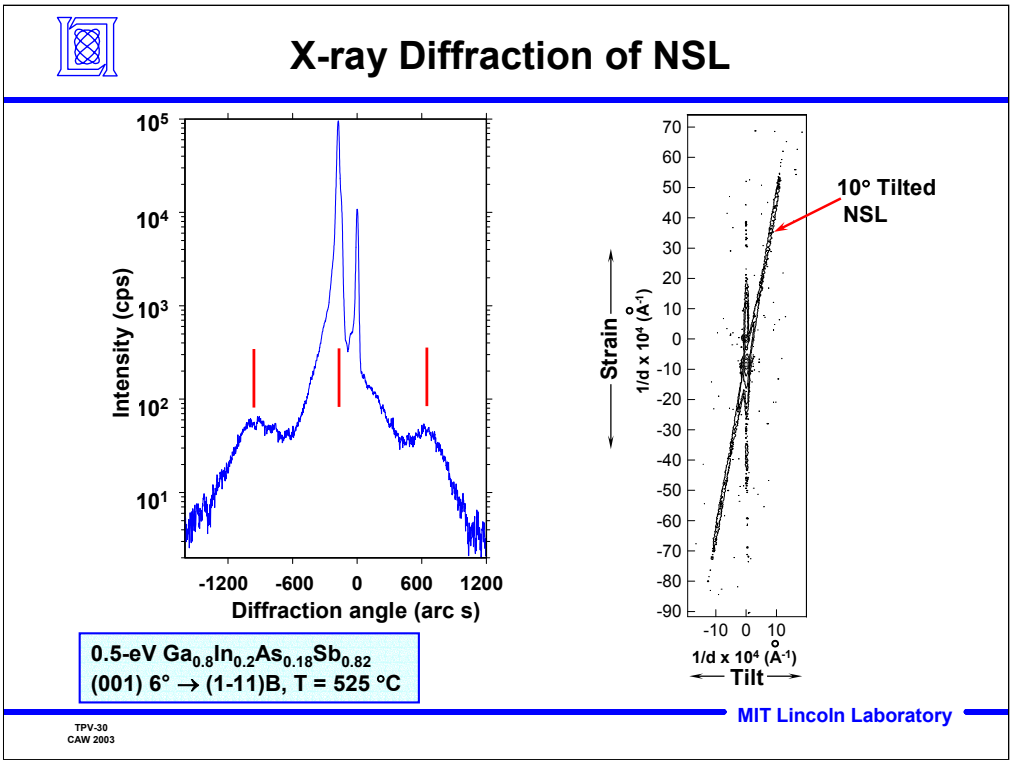

Viewgraph 30:

The NSL was also detected in XRD. The rocking curve on the left shows satellite peaks that are symmetric about the epilayer peak. The reciprocal space map on the right shows the tilted superlattice. The tilt angle can be quantitatively measured in XRD.

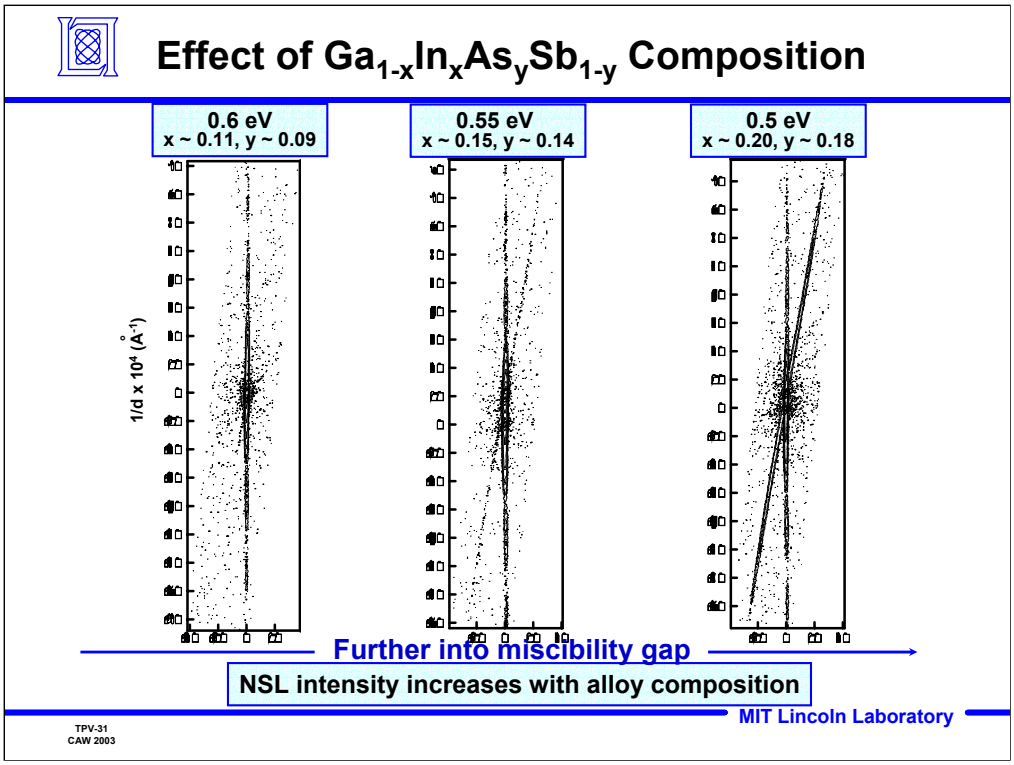

Viewgraph 31:

The reciprocal space maps of three different GaInAsSb alloys show that the intensity of the tilte superlattice increases for the alloys further into the miscibility gap.

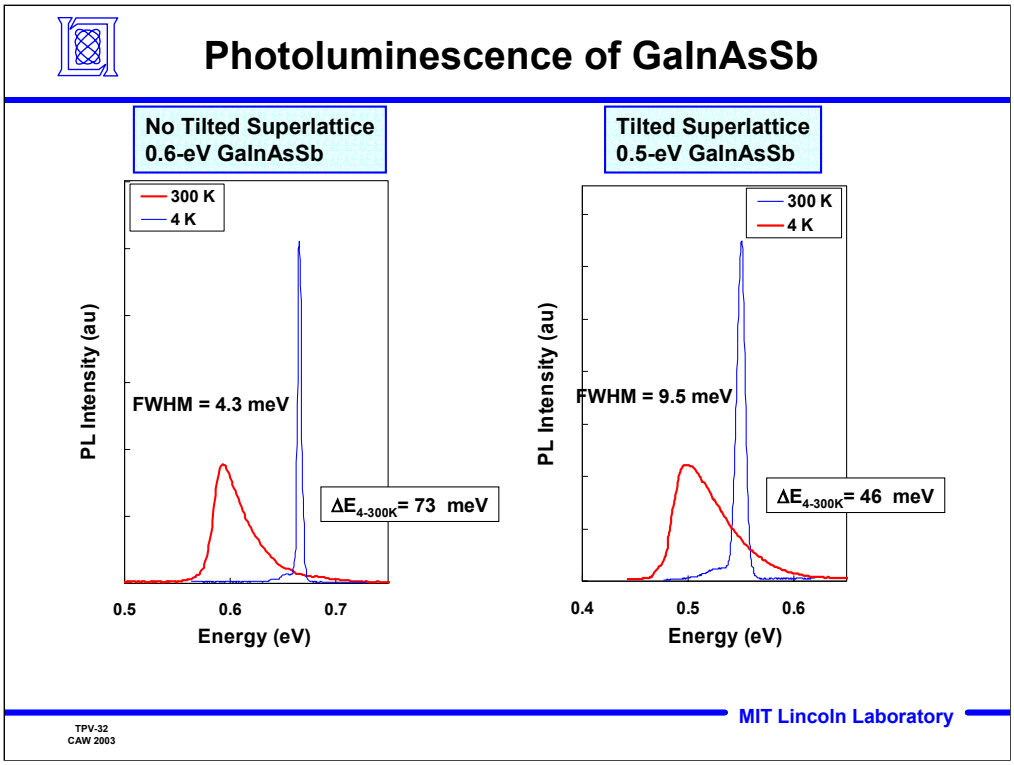

Viewgraph 32:

The microstructure can impact the electro-optical properties of GaInAsSb epilayers. Although composition modulation is expected to increase the PL linewidth because of local variations in alloy composition, the FWHM broadening was minimal as shown in this viewgraph. The sample with weak superlattice contrast has excellent PL properties and the dependence of the PL peak energy on temperature is typical of bulk materials or superlattices with a type-I band alignment.

The sample with strong superlattice contrast exhibits slight FWHM broadening which may also be due to layer thickness variations of the superlattice or spinodal decomposition. The temperature dependence of PL peak energy is similar to what is observed for type-II band alignment.

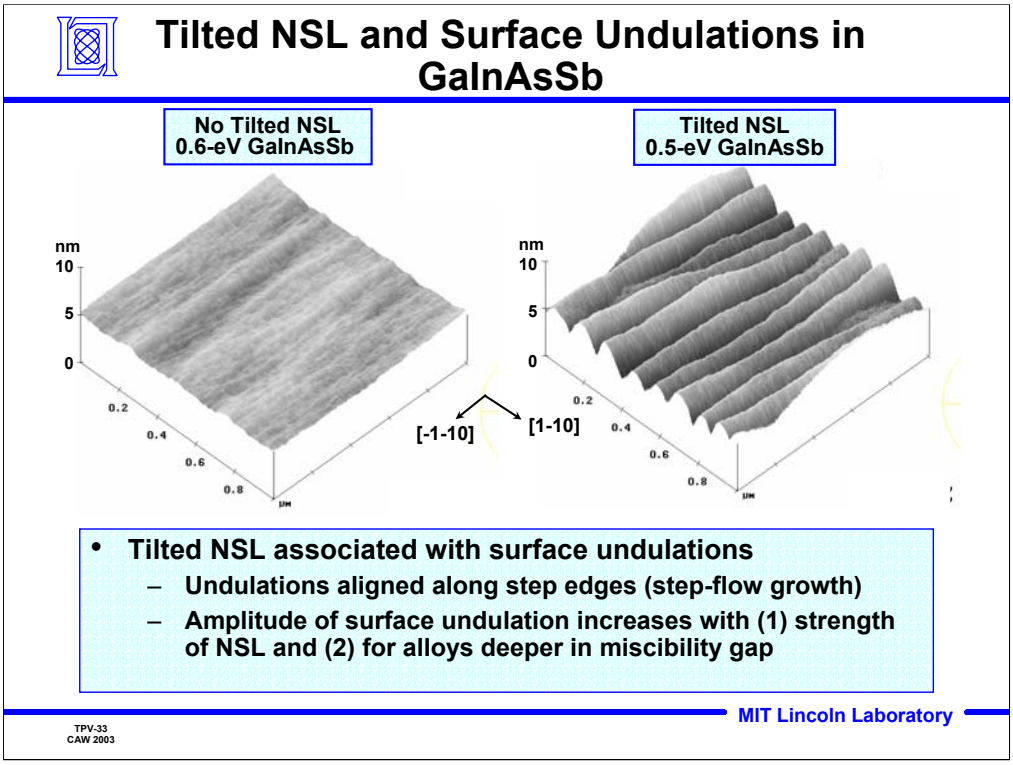

Viewgraph 33:

The existence of the tilted NSL was also correlated with surface undulations. Epilayers that did not have the tilted NSL were smooth with surface roughness of typically 2-3 nm, while those with a tilted NSL exhibited periodic surface undulations that are aligned with the step edges of the vicinal substrates. The amplitude of surface undulations increased for alloys further into the misciblity gap. Tilted NSLs were also observed on step-bunched surfaces.

Surface Undulations Coupled to Tilted Superlattice

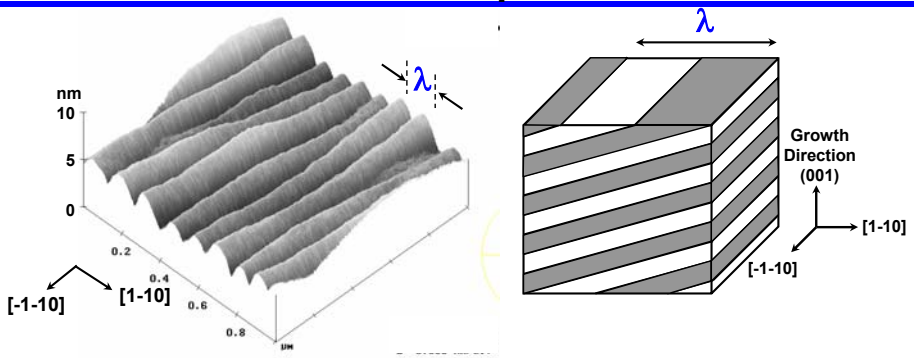

Miscut ∠	NSL period (nm)	NSL Tilt ∠	Calc λ (nm)	AFM λ (nm)
6° (1-11)B	20	10°	115	111
2° (1-11)B	14.6	5.8°	144	143
2° (101)	13.8	6.0°	132	160
2° (111)A	30	0°	∞	No undulation

Viewgraph 34:

The undulation period matches the lateral period of the 10° tilted superlattice when it intersects the surface. Furthermore, data from additional samples indicate that the amplitude of the undulations increases as the alloy composition goes further into the miscibility gap. This suggests that the undulations form on the surface to relieve the local strain from the composition modulation associated with the superlattice. This phenomenon of coupling of compositional and morphological instabilities is well documented in the literature.

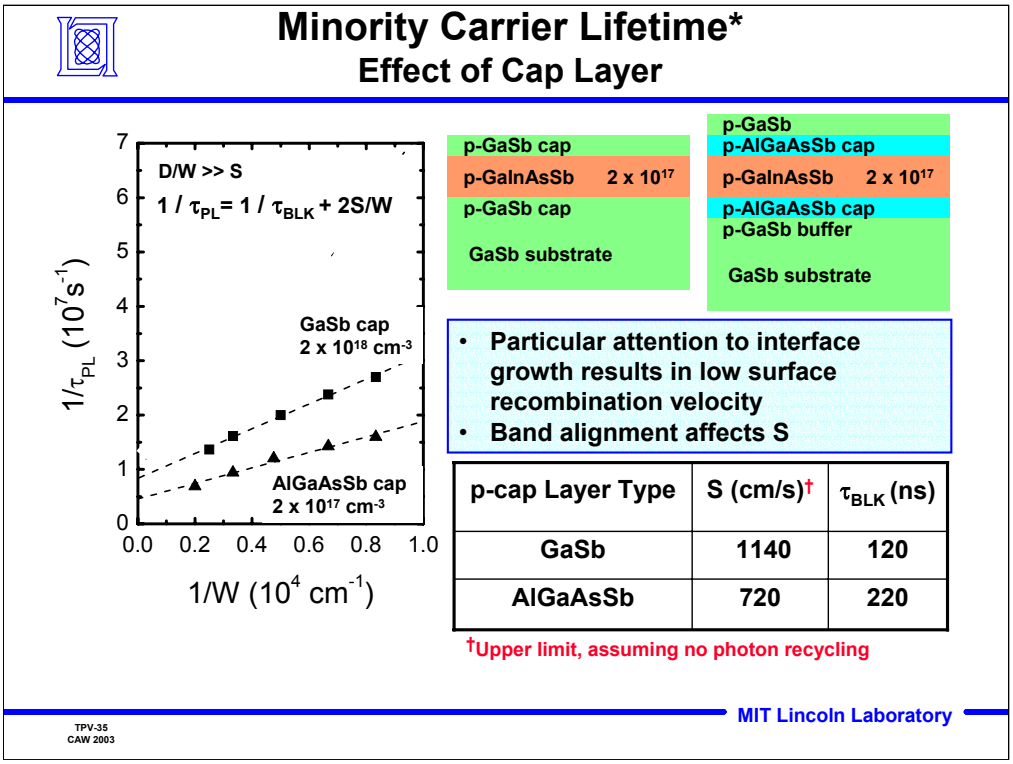

Viewgraph 35:

Minority carrier lifetime of specially grown structure were measured by time-resolved PL at Stonybrook. This viewgraph shows the dependence of $1/\tau_{PL}$ on $1/W$ for GaInAsSb heterostructures with different cap layers. All three plots demonstrate a linear dependence consistent with the equation. The structures with undoped (p = 1 x 10^{16} cm^{-3}) GaSb cap layers resulted in the highest S of 3100 cm/s. In structures with p-GaSb cap layers doped to 2 x 10^{18} cm^{-3}, S was substantially smaller at 1140 cm/s. Thus, the use of a heavily doped cap layer makes it possible to suppress interfacial recombination. S was further reduced to 720 cm/s for structures with AlGaAsSb cap layers. The smallest S was 380 cm/s for undoped GaInAsSb with AlGaAsSb cap layers.

Minority Carrier Lifetime*
Effect of GaInAsSb Doping

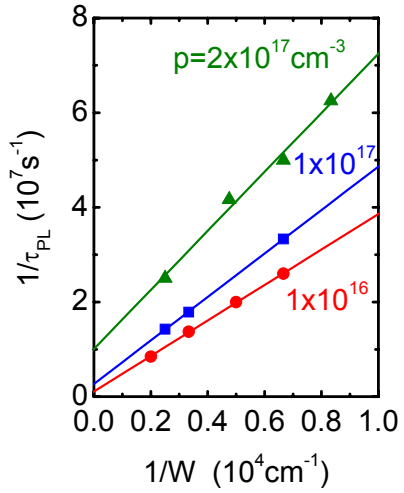

p-GaSb cap	1 x 10^{16}
p-GaInAsSb	p-varied
p-GaSb cap	1 x 10^{16}
GaSb substrate	

D/W >> S $1 / \tau_{PL} = 1 / \tau_{BLK} + 2S/W$

GaInAsSb doping (cm^{-3})	S (cm/s)	τ_{BLK} (ns)
2 x 10^{17}	3100	100
1 x 10^{17}	2300	370
1 x 10^{16}	1900	900

MIT Lincoln Laboratory

TPV-36
CAW 2003

Viewgraph 36:

The electron lifetime of p-GaInAsSb doped at various levels was measured by time resolved PL. Heterostructures with different GaInAsSb thicknesses were grown with nominally undoped p-GaSb buffer and capping layers in order to separate the contributions of bulk and interfacial recombination processes. Due to the fast electron diffusion, $D/W >> S$, the commonly used expression shown above was employed. Plotting the inverse PL decay versus inverse structure thickness reveals a linear dependence with a slope of $2S$.

The plot on the left shows the data for structures with different doping levels in the GaInAsSb layer: 1 x 10^{16}, 1 x 10^{17} and 2 x 10^{17} cm^{-3}. The radiative part of recombination depends on W due to the effect of reabsorption (photon recycling) and therefore contributes to the measured slope and affects the offset value. For structures with p = 1 x 10^{16} cm^{-3} the contribution of the photon recycling is negligible, so the offset of 900 ns for undoped structures can be used as a lower estimate of the non-radiative bulk lifetime. The results shown in the table indicate that S increases with doping in the GaInAsSb layer. These changes are related to the accumulation of electrons near the GaSb/GaInAsSb interface.

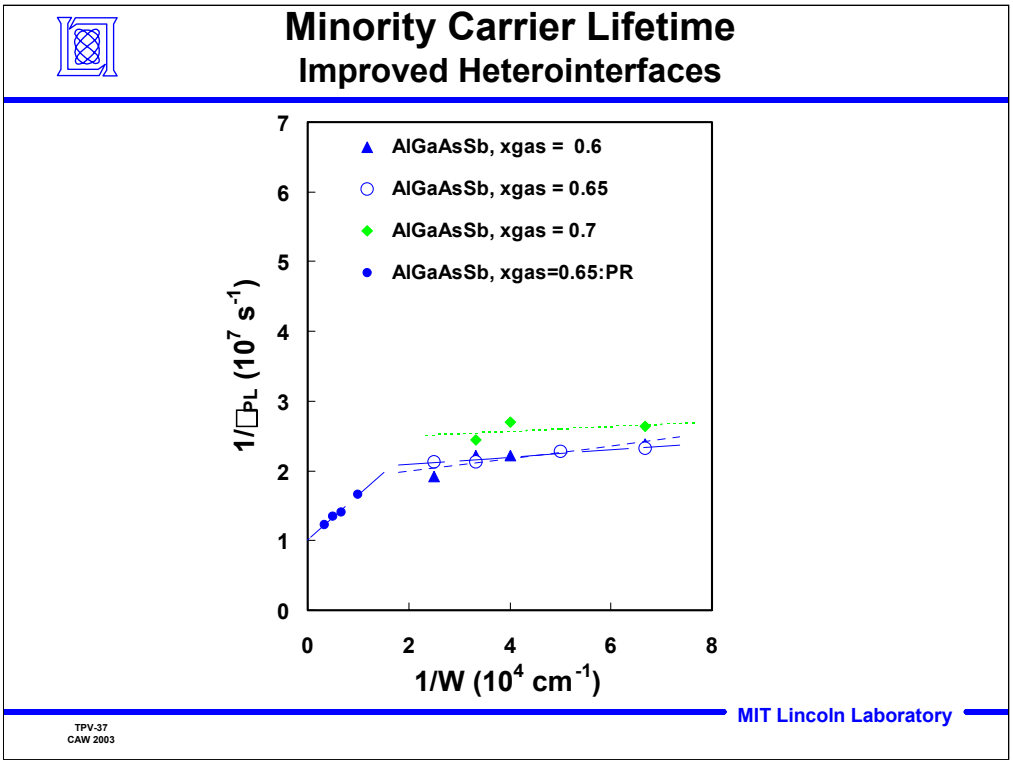

Viewgraph 37:

This viewgraph shows the most recent minority carrier lifetime results. In these samples, the growth procedures were modified to minimize growth interruptions at the heterointerfaces, and *S* has recently been measured to be as low as 30 cm/s

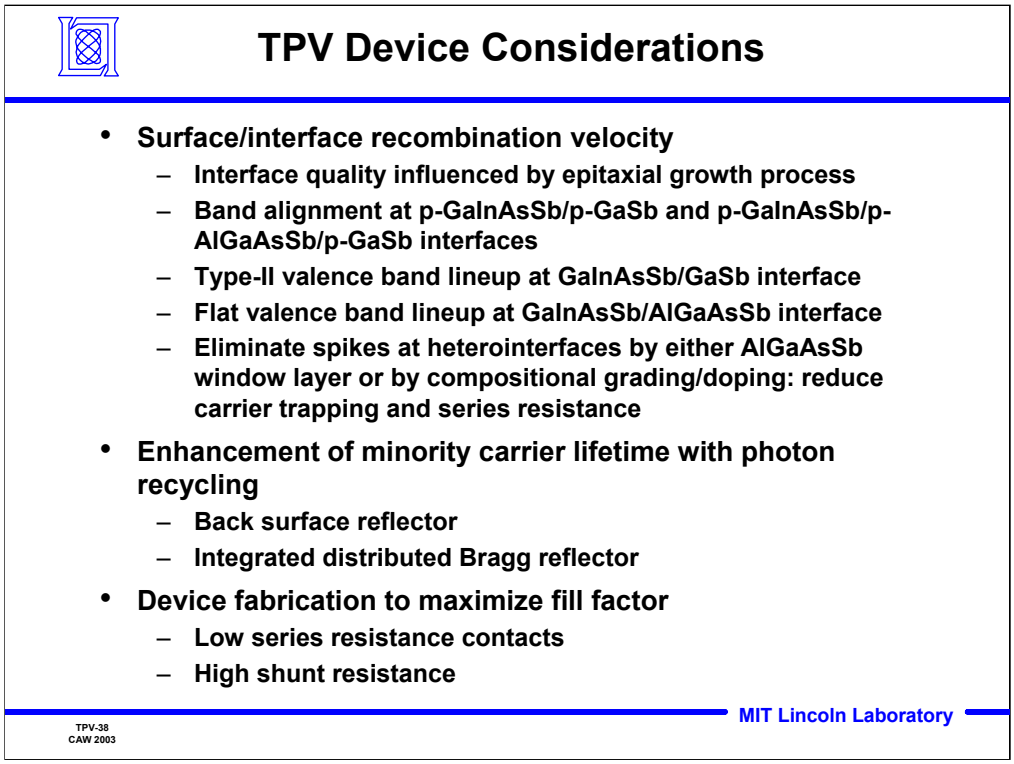

Viewgraph 38:

The SRV is a measure of the interface quality and should be minimized to increase quantum efficiency and reduce dark currents. Interface quality can be extremely sensitive to the epitaxial growth procedures. Growth studies revealed that the GaInAsSb surface is reactive at the growth temperature, but it can be stabilized under proper conditions.

Although SRV is not a fundamental property, it can also be affected by band alignment at the GaInAsSb/GaSb or GaInAsSb/AlGaAsSb interface.Type-II alignment in the p-GaInAsSb/p-GaSb interface results in a barrier to majority carrier transport and may also increase series resistance of the device. The valence bands can be lined up for the GaInAsSb/AlGaAsSb interface. Current work is underway to evaluate the subtle differences in interface growth and band alignments.

Increases in minority carrier lifetime are beneficial for TPV cell performance, and can be achieved through photon recyling. Two approaches are being studied: the use of either a back surface reflector or an integrated Bragg reflector (DBR). Substrate absorption can reduce the effectiveness of a back surface reflector, while increased series resistance can be problematic with DBR structures. Preliminary results on integrating a DBR with the TPV device are discussed.

For either approach, low series resistance contacts and high shunt resistance are critical for maximizing the fill factor.

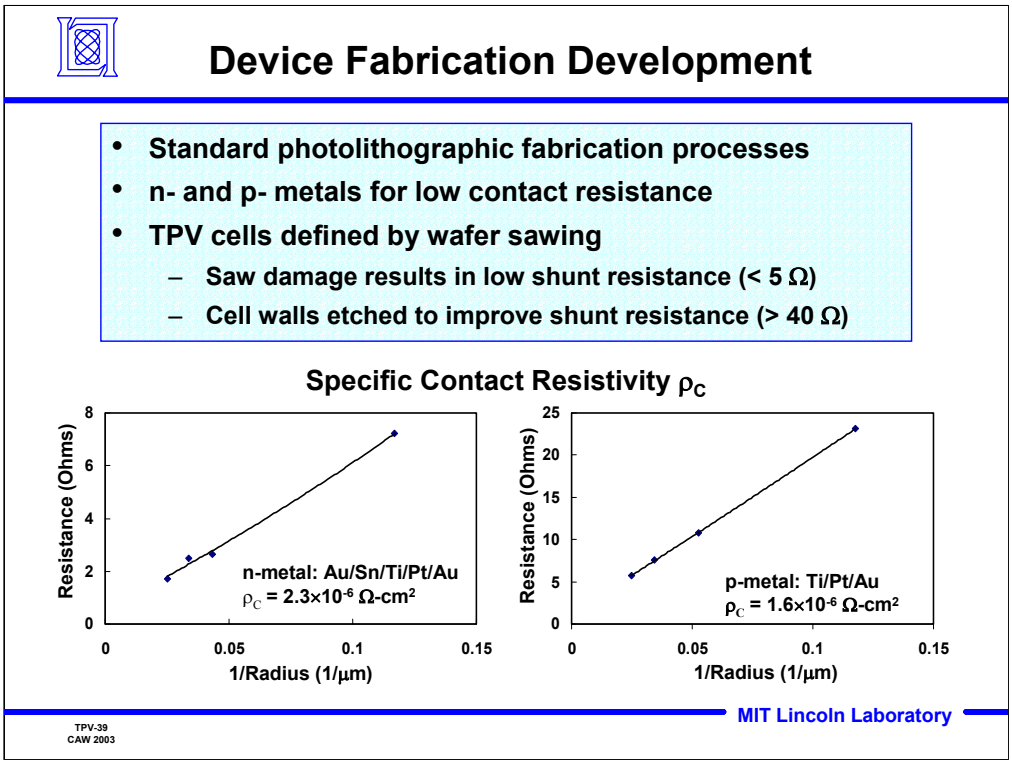

Viewgraph 39:

The specific contact resistivity (ohm-cm^2) for both the n- and p-metallization on GaSb was measured by the Cox-Strack method. It was found that both the n and p metallizations were in the low 10^{-6} ohm-cm^2 range. The specific contact resisitivity is slightly lower in the p-metallization than in the n-metallization because the Fermi level is pinned close to the valence band edge in p-GaSb.

For ease of cell fabrication, individual devices are formed by wafer sawing. The cutting introduces significant damage to the side wall of devices and results in very low shunt resistance and degradation of the fill factor.

Saw-cut damage can be removed with sufficient material etching, as was observed in SEM micrographs of the sidewall before and after etching. The shunt resistance could be increased from a few ohms to hundreds of ohms, while the fill factors increased from below 60% to 70%.

TPV Device Structure Improvements

- Back surface reflectors (BSR) to increase effective optical thickness and enhance photon recycling
  - Improve long wavelength spectral response, V_{oc}
- BSRs on n-GaSb limited by free-carrier absorption
- Integrated distributed Bragg reflector (DBR): narrow band

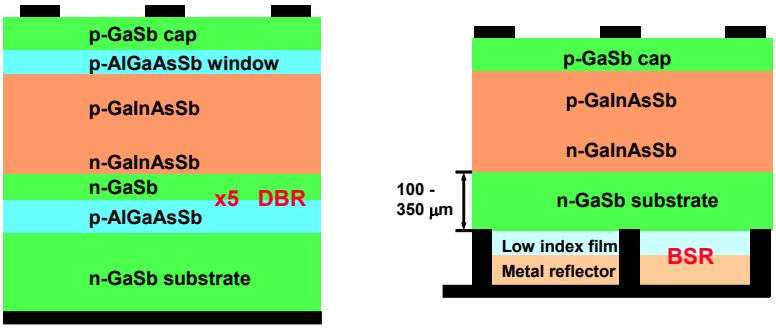

Viewgraph 40:

Two approaches for improving TPV cell performance use a reflector structure, and are shown in this viewgraph. It is expected that the reflector will increase minority carrier lifetime through photon recyling and will provide double-pass absorption for photons that are not absorbed in the first pass. The approach on the left incorporates and integral quarter-wave distributed Bragg reflector (DBR), while the approach on the right is a hybrid ohmic contact back-surface reflector (BSR) deposited on the back of the GaSb substrate. The DBR is more growth intensive, while the and BSR is more fabrication intensive.

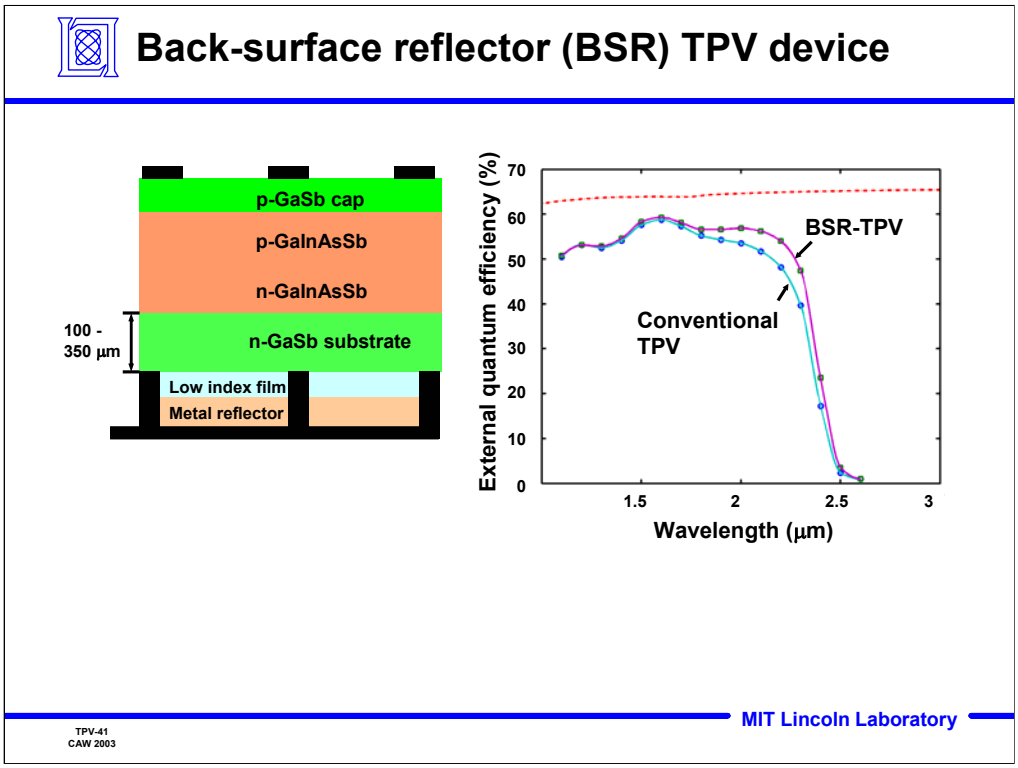

Viewgraph 41:

The EQE of an uncoated BSR-TPV device with substrate thickness of about 120 microns is shown on the left graph. For comparison, the EQE of a conventionally processed TPV cell from the same is also shown. The solid lines are guides for the eyes. The reflection limit of GaSb is also shown, in the dotted-dashed line. In the wavelength regime from about 1.1-μm to 1.7-μm, the BSR-TPV cell and the reference cell have approximately the same EQE since the GaSb substrate is absorbing below 1.7 μm. From about 1.7-μm to 2.5-μm, the EQE of the BSR-TPV cell exceeds that of the reference cell, and indicates the enhancement due to the double-pass absorption. This comparison is made more clear in the graph on the right, in which the difference in EQE is plotted. This value, $\Delta EQE(\lambda)$ is equal to $EQE_{BSR\text{-}TPV}(\lambda) - EQE_{REF\text{-}TPV}(\lambda)$, where $EQE_{BSR\text{-}TPV}(\lambda)$ and $EQE_{REF\text{-}TPV}(\lambda)$ are the external quantum efficiencies of the BSR-TPV cell and the reference TPV cell, respectively. The peak difference in EQE is about 8% at a wavelength of 2.35-μm, which corresponds to a fractional increase in EQE of about 20% at this wavelength.

DBR TPV

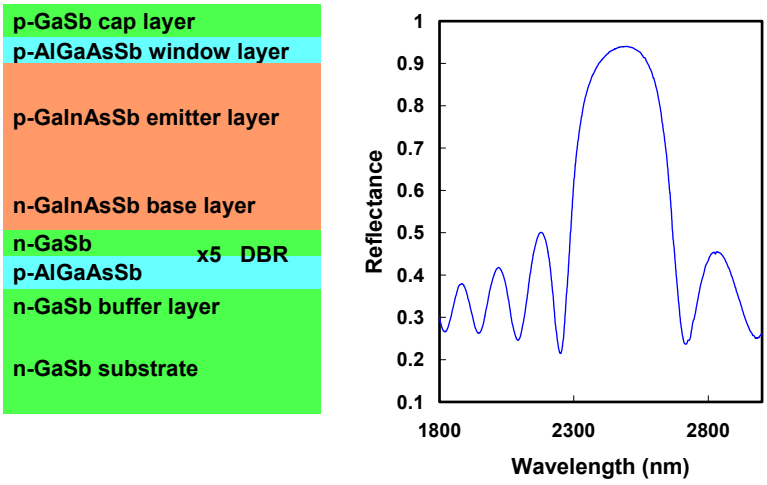

Viewgraph 42:

A TPV device structure was grown with a 5- period DBR structure. The reflectance spectra on the right is for a 10-period DBR. The narrow reflectivity band should enhance the near-band-edge performance.

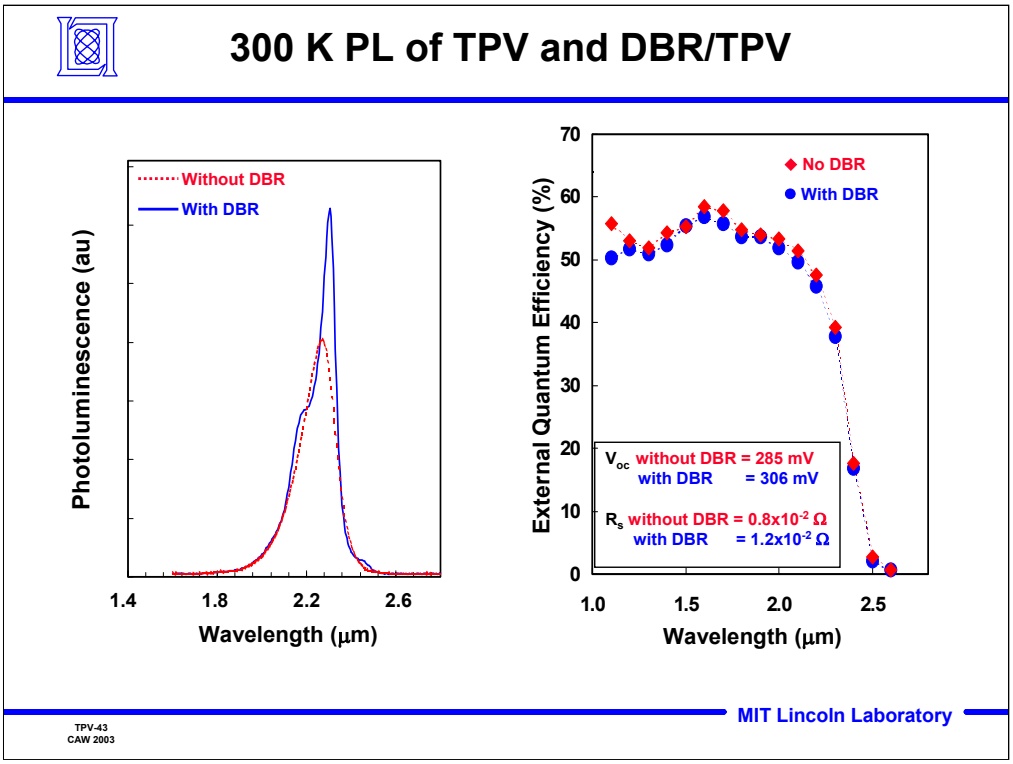

Viewgraph 43:

The 300 K PL spectra for the TPV control structure and the DBR/TPV structure are compared in this viewgraph. The PL intensity is significantly increased due to photons reflecting off the DBR. The reflectance from the structure with the DBR i ncreases by about 40%.

The EQE of the uncoated TPV and DBR/TPV structures shows similar performance, since the reflection is centered at 2400 nm. It is expected that increased efficiency may be obtained for reflection centered at 2000 nm. The V_{oc} increased by about 7%. Assuming no other changes in the device parameters, the photon recyling factor is estimated to be about 2.5.

The series resistance for the TPV cell with the DBR is slightly higher. Grading the interfaces in the DBR structure should reduce the series resistance.

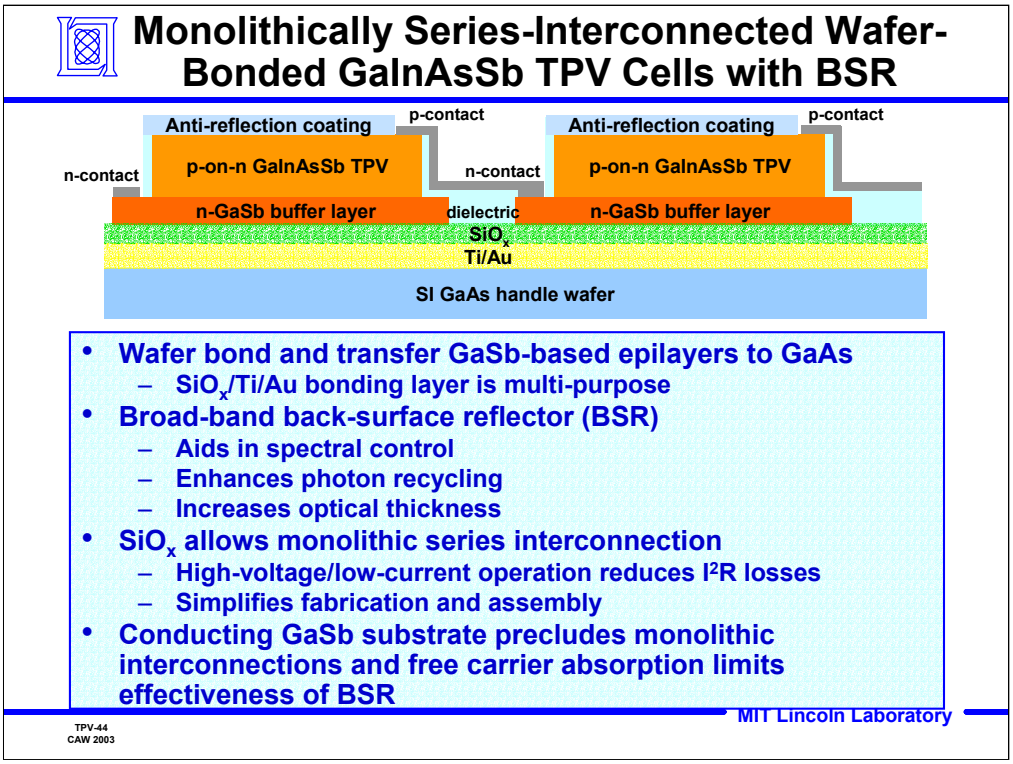

Viewgraph 44:

It may also be of interest to monolithically integrate TPV devices and connect them in series, as is being done for InGaAs/InP devices. Such an approach requires that the epitaxial structure be on an electrically insulating substrate. Since GaSb substrates can not be made electrically insulating at room temperature, alternative approaches are required.

Two possible approaches are 1) growth on an isolation layer or cell isolation diode and 2) epitaxial layer transfer to an insulating substrate. The second approach is schematically shown. There are several variations to this approach in which the bonding layer can be an oxide, metal, or composite oxide/metal layer. Alternatively, a bonding layer is not used and the GaSb is atomically bonded to GaSb. In this case, the TPV structure would be grown on an atomically bonded GaSb 'buffer' layer.

At present, device processing for monolithic integration has to be refined, while electrical isolation approaches are being developed.

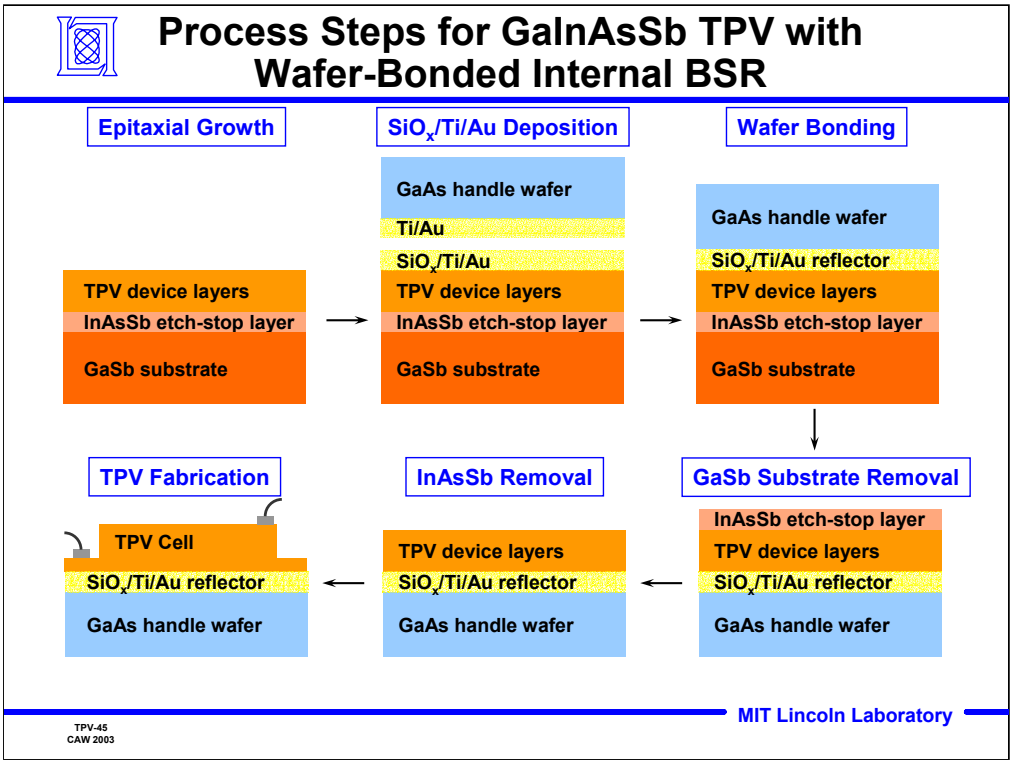

Viewgraph 45:

The process steps for fabrication of wafer-bonded TPV devices is shown in this viewgraph. We recently have developed the complete process, and will present results of the materials and devices.

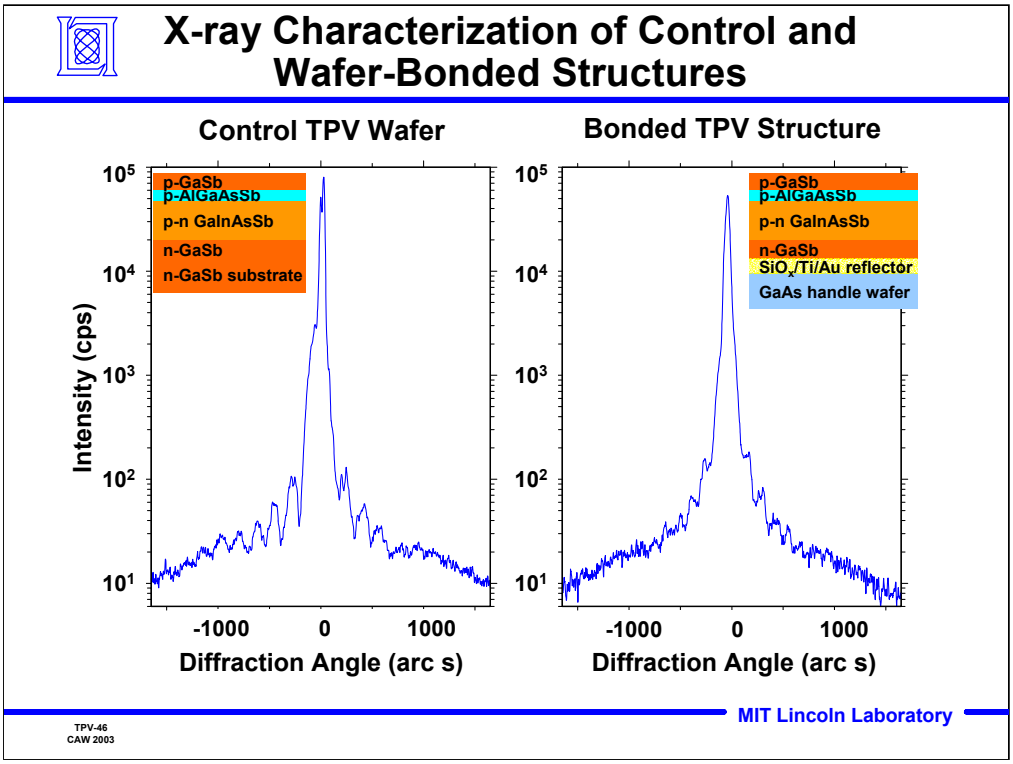

Viewgraph 46:

This viewgraph shows a comparison of the XRD rocking curves for a control TPV wafer and a wafer-bonded TPV structure. The diffraction intensity is lower for the bonded TPV device structure since the GaSb substrate has been removed and only the epitaxial layers that were grown lattice-matched to GaSb are remaining. The diffraction peak of the bonded epitaxy is only slightly broadened with full-width at half-maximum (FWHM) of 51 arc s, compared to that of the control structure with FWHM of ~30 arc s. The observation of thickness fringes in both samples is indicative of the excellent structural quality and minimal wafer curvature.

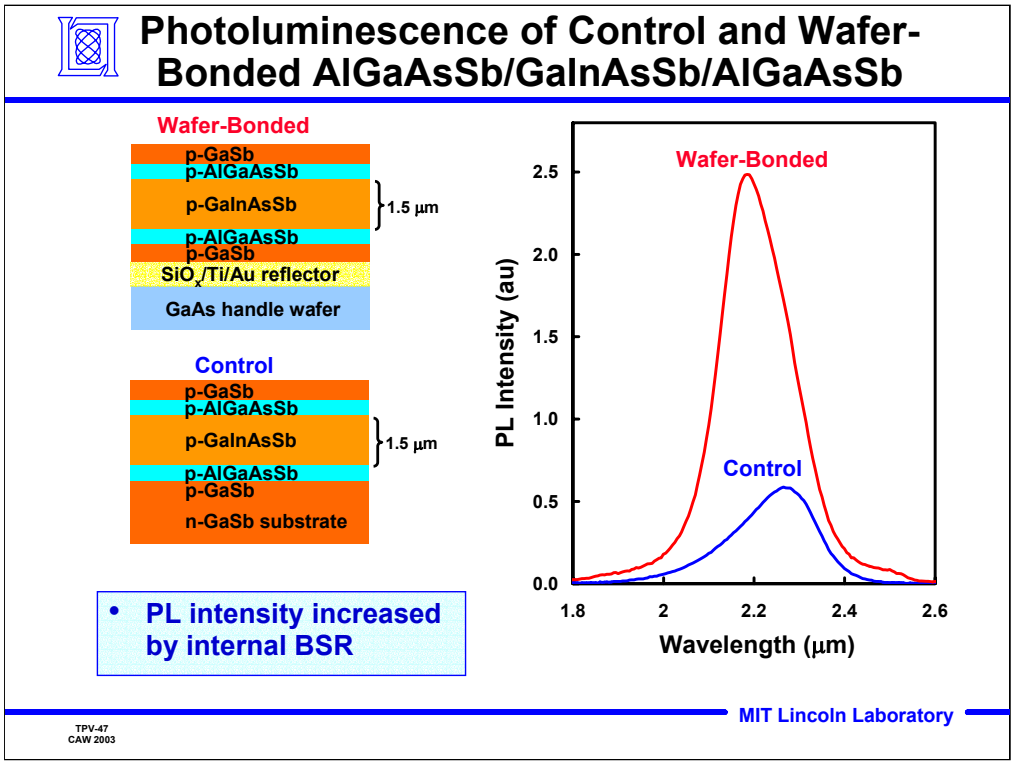

Viewgraph 47:

A comparison of the 300 K PL intensity of a control and wafer-bonded lifetime structure are shown in this viewgraph. The PL peak intensity of the wafer-bonded structure with the internal BSR is almost five times greater than that of the control structure. These results suggest that the optical efficiency is enhanced as a result of the internal BSR, and thus there is negligible material degradation after wafer bonding and substrate removal.

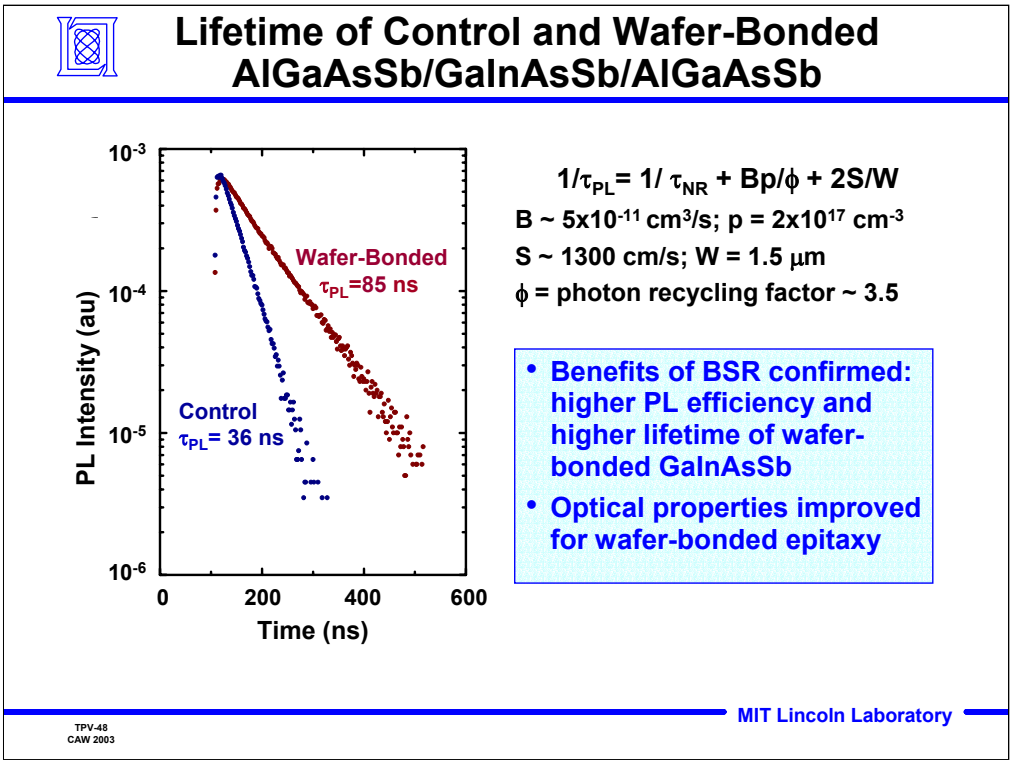

Viewgraph 48:

Time-resolved photoluminescence measurements were made to extract minority-carrier lifetime of p-GaInAsSb doubly capped with AlGaAsSb. The lifetime measured by PL decay is more than two times higher at 85 ns for the WB sample with the internal BSR compared to the control sample with decay time of 40 ns. These results show that photons that might normally be absorbed in the substrate are reflected back to the active layer and reabsorbed, and the internal BSR is effective in increasing minority-carrier lifetime. The minority carrier lifetime was also compared. The enhancement in lifetime for the wafer-bonded sample is indicative of the enhancements due to photon recycling.

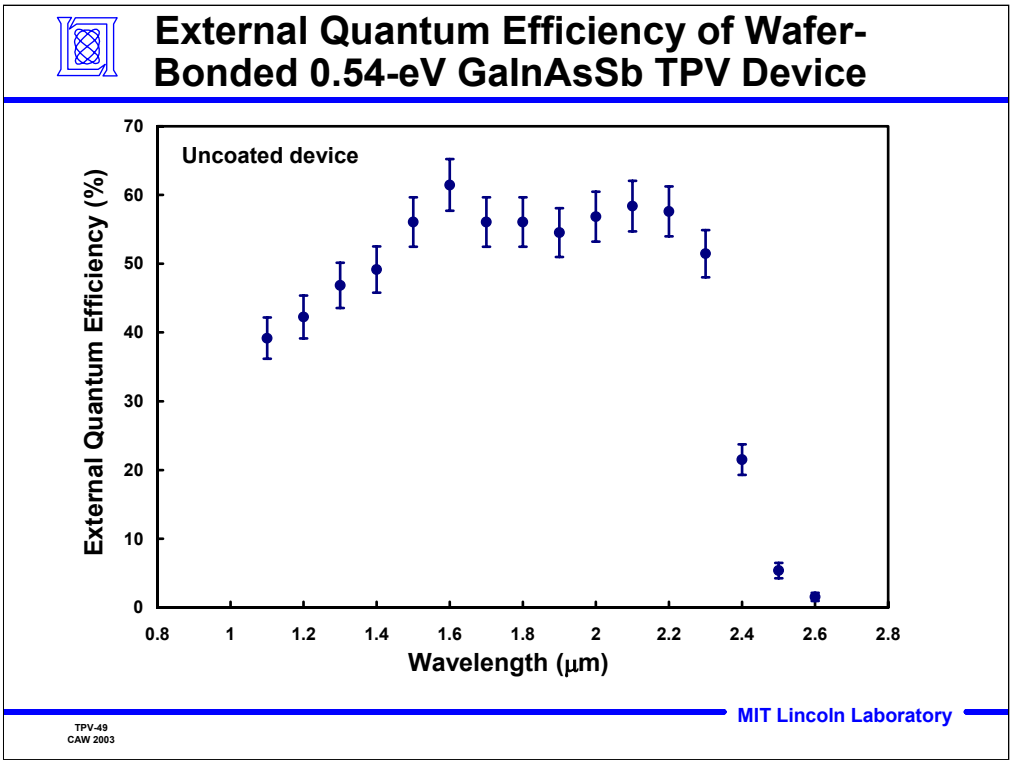

Viewgraph 49:

The external quantum efficiency of a wafer-bonded and uncoated TPV device is shown. The efficiency is slightly lower compared to conventional TPV devices, but is very encouraging nevertheless.

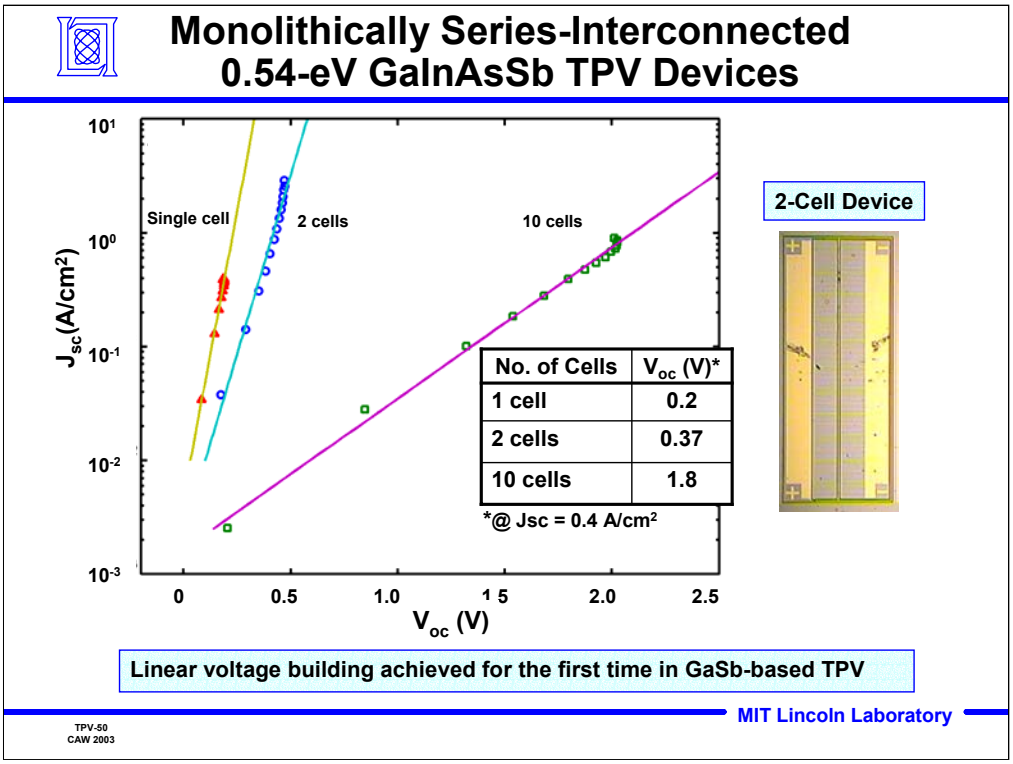

Viewgraph 50:

This viewgraph shows the short-circuit current density J_{sc} versus V_{oc} for a single-junction TPV cell and 2- and 10-junction series-interconnected TPV cells that were fabricated on the wafer-bonded material. At J_{sc} ~ 0.4 A/cm2, the single cell exhibits V_{oc} ~ 0.2 V. At this same current density, V_{oc} is 0.37 and 1.8 V for the 2- and 10-junction devices, respectively. These results indicate that nearly linear voltage building has been achieved. At higher J_{sc} ~ 1 A/cm2, V_{oc} is ~ 0.470 and 2.0 V for the 2- and 10-junction devices, respectively. The saturation of V_{oc} at high Jsc levels may be due to heating of the devices, which were not mounted on a heatsink. The V_{oc} for the single cell is slightly lower compared to previously reported values for conventional TPV cells, and is likely related to a higher saturation current. This may stem from the larger cell perimeter/area ratio compared to previously reported cells or from pinholes in the epitaxy due to etching. The fill factor FF of the 2-junction device is about 51% at Jsc ~ 0.4 A/cm2, and degrades to about 38% at Jsc ~ 1 A/cm2. This degradation is related to high series resistance in the cell-to-cell interconnections, and could be reduced with improved metallization and reduced resistance in the n-GaSb lateral conduction layer.

Summary

- **Epitaxial growth and fabrication studies directed toward improving GaInAsSb/AlGaAsSb/GaSb TPV device performance**
- **IQE and FF approaching theoretical limits, V_{oc} within 12%**
- **Back-surface reflector designs evaluated for further enhancements**
  - **Integrated DBR/TPV device exhibits higher open circuit voltage**
  - **TPV with back-surface reflector exhibits higher quantum efficiency near GaInAsSb band edge**
- **Alternative approach by wafer-bonding for monolithic interconnection of GaSb-based TPVs**

Viewgraph 51:

This presentation has discussed the development of GaInAsSb materials and device structures for lattice-matched TPV devices. The performance of TPV cells is approaching theoretical limits. These TPV devices can routinely be fabricated, indicating good control and reproducibility of both epitaxial growth and device processing. Preliminary results on devices with an integral DBR structure indicate an increase in V_{oc}. Improvements in EQE was measured for TPV cells with a BSR. Initial results of wafer-bonded TPV devices are very encouraging.